Orientation-angle-resolved photoelectron angular distribution in dissociative ionization of methanol induced by an intense ultraviolet laser pulse

Shinichi Fukahori [1,2,3,4] Tomohito Otobe,[1] Hiroshi Akagi [1] Kaoru Yamanouchi [2] and Ryuji Itakura [1,*]

[1]*Kansai Photon Science Institute, National Institutes for Quantum Science and Technology (QST),*
8-1-7 Umemidai, Kizugawa, Kyoto 619-0215, Japan
[2]*Department of Chemistry, School of Science, The University of Tokyo, 7-3-1 Hongo, Bunkyo-ku, Tokyo 113-0033, Japan*
[3]*Department of Integrated Sciences, Graduate School of Arts and Sciences, The University of Tokyo,*
3-8-1 Komaba, Meguro-ku, Tokyo 153-8902, Japan
[4]*Komaba Institute for Science, Graduate School of Arts and Sciences, The University of Tokyo,*
3-8-1 Komaba, Meguro-ku, Tokyo 153-8902, Japan

We investigate dissociative ionization of methanol, $CH_3OH \rightarrow CH_3^+ + OH + e^-$, in a linearly polarized intense ultraviolet laser field (400 nm, 67 fs, 3.1×10^{13} W/cm^2) by photoelectron-photoion coincidence three-dimensional momentum imaging. The photoelectron angular distributions (PADs) are recorded as a function of the orientation angle between the molecular C-O bond axis and the laser polarization direction. Photoelectrons are emitted dominantly along the laser polarization direction when CH_3OH^+ is produced in the $\tilde{X}$ state via the four-photon absorption. By contrast, the photoelectron emission becomes prominent along the direction perpendicular to the laser polarization direction when CH_3OH^+ is produced in the $\tilde{B}$ state via the five-photon absorption. The orientation-angle-resolved PADs are expanded in terms of spherical harmonics in the laboratory frame, and then the anisotropy of the PADs varying as a function of the orientation angle of the C-O bond axis with respect to the laser polarization direction is examined quantitatively. We discuss how the shape of the molecular orbital from which an electron is emitted is reflected in the recorded PADs.

I. INTRODUCTION

When molecules are exposed to an intense laser field, a variety of dynamical processes such as molecular dissociation [1,2], high-order harmonic generation [3,4], and multiple ionization [5] are induced and associated with photoelectron emission. In the strong field limit, a photoelectron tunnels through the barrier of the distorted Coulomb potential along the laser electric field (***E*** field), and the freed electron is driven by the subsequent ***E*** field. Therefore, when the laser polarization is linear, the final photoelectron momentum $\boldsymbol{p}_{\text{elec}}$ becomes parallel to the ***E*** field. In the weak field limit where only one-photon absorption is possible, the photoelectron angular distribution (PAD) can be described well in the molecular frame (MF) independent of the direction of the ***E*** field, and consequently, the amplitude and phase of the photoionization transition matrix elements can be evaluated from the molecular-frame PADs (MF-PADs) [6–10].

However, as the laser field intensity increases, the MF-PAD starts exhibiting dependence on the alignment or orientation angle between the molecular axis and the ***E*** field. Therefore, the ionization process cannot be characterized by the MF-PAD unless the molecular alignment or orientation with respect to the ***E*** field is specified. In this study we focus on the photoelectron emission processes of molecules in the intermediate laser field intensity range of 10^{12}–10^{13} W/cm^2. In the case

of polar molecules, we need to reveal the variation of a MF-PAD as a function of the orientation angle of the molecular axis with respect to the ***E*** field, which is called hereafter an orientation-angle-resolved (OR) PAD.

In the intermediate laser field intensity range, the alignment dependence of the photoelectron images was investigated by the velocity map imaging method for CS_2 [11], N_2, CO_2, and C_2H_4 [12] and by cold target recoil ion momentum spectroscopy for H_2 [13]. In these studies the dependence of the PAD on the extent of the molecular alignment was investigated by assuming that the MF-PADs are cylindrically symmetric with respect to the laser polarization axis even though this assumption is not always valid. Therefore, the dependence of the MF-PADs on the molecular orientation needs to be examined.

In our previous study [14], by the photoelectron-photoion coincidence (PEPICO) three-dimensional (3D) momentum imaging method, we recorded MF-PADs for dissociative ionization of methanol ($CH_3OH \rightarrow CH_3^+ + OH + e^-$) in a linearly polarized ultraviolet (UV) laser field (398 nm, 8.9×10^{12} W/cm^2). By taking advantage of the fact that the UV photon energy is large enough to separate electronic states of methanol ions in the photoelectron spectrum, we revealed that the direction of the photoelectron emission tends to be parallel to the CH_3^+ recoil direction for the four-photon ionization to the $\tilde{X}$ state of CH_3OH^+ with the subsequent excitation to higher-lying states above the dissociation threshold, while it tends to be perpendicular for the five-photon ionization to the $\tilde{B}$ state. In addition, for the ionization to the $\tilde{B}$ state,

*itakura.ryuji@qst.go.jp

we revealed that the yield of photoelectrons emitted in the direction from the carbon (C) atom to the oxygen (O) atom is larger than that in the direction from the O atom to the C atom. However, because the number of the accumulated events was not sufficiently large to obtain the orientation dependence of the MF-PADs, we obtained the MF-PADs averaged over the orientation angle to discuss the dissociative ionization pathways of methanol in the UV laser field.

In the present study we investigate photoelectron emission dynamics of methanol by accumulating a sufficiently large number of coincidence events to extract the MF-PAD as a function of the orientation angle defined as the angle between the laser polarization direction and the molecular axis. On the basis of the OR-PADs obtained using the PEPICO 3D momentum imaging method, we reveal that the OR-PADs are not cylindrically symmetric with respect to the laser polarization axis and that multiphoton and tunneling ionization processes compete. Furthermore, we discuss how the shape of the molecular orbital from which an electron is emitted is reflected to the resultant OR-PAD when the laser field intensity is in the intermediate regime.

II. EXPERIMENT

Linearly polarized UV laser pulses (400 nm, 67 fs, 0.1 mJ/pulse, 1 kHz) obtained by the frequency doubling of output pulses of a Ti:sapphire amplifier system with a β-barium borate crystal (0.2 mm thick, type I) are focused by an uncoated aluminum off-axis parabolic mirror ($f = 200$ mm) on an effusive molecular beam of a pure methanol (CH_3OH) vapor at right angles in an ultrahigh vacuum chamber (base pressure $\sim 2 \times 10^{-8}$ Pa). By the adjustment of the diameter of the UV beam using an iris, the laser-field intensity at the interaction point is set to be 3.1×10^{13} W/cm^2, which is estimated from the ponderomotive energy shift of 0.46 eV in the photoelectron energy spectrum of Xe. This estimated intensity is regarded as that averaged over the volume around the focal point. The focal spatial profile is imaged onto a charge-coupled device (CCD) camera using a plano-convex lens (synthetic fused silica, $f = 166.32$ mm at 400 nm) with a magnification of 3.1 and is measured to be 9 μm radius at the $1/e^2$ intensity. The diffraction fringe is not identified in the recorded image. The corresponding Rayleigh length is estimated to be 0.6 mm. Because the PADs recorded in the present study is almost the same as those recorded at the different laser field intensity of 8.9×10^{12} W/cm^2 in our previous study [14], the influence of the focal volume averaging on the PAD pattern is considered to be negligibly small.

A photoelectron and a photoion generated in each laser shot at the focal point are extracted to the opposite directions, both of which are perpendicular to the laser propagation direction as well as to the molecular beam, and are focused respectively by electrostatic lenses on the position-sensitive detectors (RoentDek HEX80). The electric field at the focal point along the extraction directions of ions and electrons is 5.2 V/mm. The momentum resolution of electrons and ions is governed by the Rayleigh length (0.6 mm) of the focused laser beam which is half as wide as the molecular beam diameter estimated by changing the focusing position in the
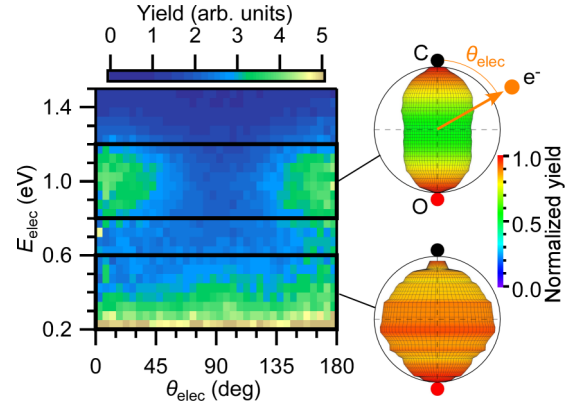
FIG. 1. Energy-resolved MF-PAD $F_E(\theta_{elec}, E_{elec})$ for CH_3^+ formation, where θ_{elec} is the angle between the momentum vector of a photoelectron and the recoil vector of CH_3^+ and E_{elec} is the photoelectron energy. The energy ranges of 0.2–0.6 eV and 0.8–1.2 eV are assigned to the five- and four-photon ionization to the $\tilde{B}$ and $\tilde{X}$ states, respectively. The stereographic drawings of MF-PADs in the respective energy ranges are shown in the right-hand side. In these stereographic drawings, the yields are normalized by their maxima.

direction perpendicular both to the axis of the effusive beam of a methanol vapor and to the laser propagation direction. We find CH_3OH^+, CH_2OH^+, $CHOH^+$, HCO^+, and CH_3^+ as the product ion species, but we focus hereafter on the dissociation channel from which CH_3^+ is produced. The angular resolution of the CH_3^+ recoil at the kinetic energy of 0.3 eV is confirmed to be less than 3°. The angular resolution of the photoelectron emission at the kinetic energy of 0.45 and 1.06 eV is estimated to be less than 3° by taking into account the temporal resolution (25 ps) of the time-to-digital converter (RoentDek TDC8HP) in the data acquisition system. The event rates of the detection of ions and electrons are kept at around 0.3 events per laser shot to secure the coincidence detection. The 3D momentum vector of the photoelectron $\boldsymbol{p}_{elec}$ and that of the photoion $\boldsymbol{p}_{ion}$ are determined from their arrival times and two-dimensional (2D) positions on the detectors. In order to collect a sufficiently large number of coincidence events for the construction of OR-PADs, we accumulate about 1.2 million coincidence events for the CH_3^+ formation channel, which are 13 times as large as the event numbers accumulated in our previous measurements [14]. More details of the experimental setup can be found in our previous reports [2].

III. RESULTS AND DISCUSSION

A. Energy-resolved molecular-frame PAD

From the accumulated events, the energy-resolved MF-PAD $F_E(\theta_{elec}, E_{elec})$ for the CH_3^+ formation channel are extracted as shown in Fig. 1, where θ_{elec} is the angle between the momentum vector of a photoelectron, $\boldsymbol{p}_{elec}$, and the recoil vector of CH_3^+, $\boldsymbol{p}_{ion}$, and E_{elec} is the photoelectron kinetic energy. The vector $\boldsymbol{p}_{ion}$ is considered to be the direction from the O atom to the C atom, that is, parallel to the C-O bond axis of CH_3OH, under the axial-recoil approximation because the C-O bond dissociation, proceeding within 500 fs
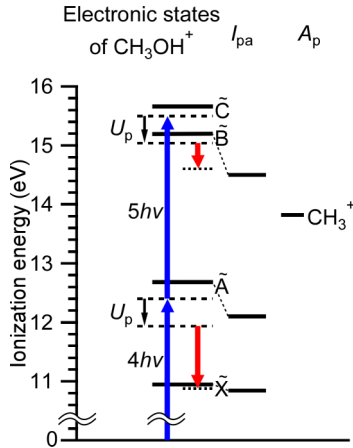
FIG. 2. Energy diagram of CH_3OH^+. The horizontal bars on the left side indicate the vertical ionization energies to the $\tilde{X}$ (10.94 eV), $\tilde{A}$ (12.68 eV), $\tilde{B}$ (15.19 eV), and $\tilde{C}$ (15.66 eV) states of CH_3OH^+ measured from the electronic ground state of CH_3OH [17]. The three horizontal bars in the center represent the adiabatic ionization energies I_{pa} of the $\tilde{X}$, $\tilde{A}$, and $\tilde{B}$ states, which are lower than the respective vertical ionization energies by 0.1, 0.6, and 0.7 eV [18]. The appearance energy A_p for the dissociation channel CH_3^+ + OH (13.82 eV) [19] is also shown on the right side. The ponderomotive energy U_p at the laser intensity of 3.1×10^{13} W/cm^2 is U_p = 0.46 eV. The respective lengths of the two vertical red arrows represent the photoelectron kinetic energies of E_{elec} = 0.45 and 1.06 eV, while the length of the vertical blue arrows represents the UV photon energy of 3.10 eV.

in the singly charged state [15], is much faster than the period of the overall rotation of CH_3OH (around 20 ps) estimated from the rotational constants, B and C [16]. Although the dynamical alignment proceeds during and after the interaction with a pulsed laser field, the axial-recoil approximation is still useful to define the C-O axis at the moment of photoelectron emission as will be quantitatively evaluated later in Sec. III D.

As shown in Fig. 1, in the energy range around E_{elec} = 1.06 eV, the photoelectron is emitted predominantly along the directions of θ_{elec} = 0° and 180°, i.e., the directions parallel to the C-O bond axis. As shown in Fig. 2, the emission of a photoelectron at E_{elec} = 1.06 eV is associated with the nonresonant four-photon ionization resulting in the formation of the electronic ground state (the $\tilde{X}$ state) of CH_3OH^+ [14] as discussed before on the basis of the energy levels of the electronic states of CH_3OH^+ [17,18]. Because the appearance energy of CH_3^+ [19] via the decomposition into CH_3^+ and OH is about 2.98 eV above the vibrational ground state of the $\tilde{X}$ state of CH_3OH^+ as shown in Fig. 2, the subsequent electronic excitation from the $\tilde{X}$ state is necessary for the formation of CH_3^+. Judging from the translational energy distribution of CH_3^+ produced via the $\tilde{X}$ state recorded in our previous study [14], CH_3^+ is produced not only via the $\tilde{B}$ state but also via the higher-lying states prepared by subsequent multiphoton absorption from the $\tilde{X}$ state. As will be discussed in Sec. III D, the effect of the alignment-angle dependent excitation probability is negligibly small so that the OR-PADs can be discussed under the axial recoil approximation.

Meanwhile, in the energy range around E_{elec} = 0.45 eV in Fig. 1, the angular distribution exhibits peaks around θ_{elec} = 90° and 180° as shown in the stereographic drawing of the MF-PAD in Fig. 1, indicating that the photoelectrons are emitted along the direction perpendicular to the C-O bond and along the direction from the C atom to the O atom, respectively. As shown in Fig. 2, the emission of a photoelectron at E_{elec} = 0.45 eV is associated with the nonresonant five-photon ionization, resulting in the formation of the second electronically excited state (the $\tilde{B}$ state) of CH_3OH^+, from which the CH_3^+ formation is energetically possible via the decomposition into CH_3^+ and OH [14].

B. Orientation-angle resolved PAD

In order to derive the OR-PADs, we sort the events according to the polar angle θ_{pol} ($0° \leqslant \theta_{pol} \leqslant 90°$) of the E-field direction measured from the C-O bond axis with the bin size of 10°. The resultant OR-PADs are not cylindrically symmetric with respect to the C-O bond axis except at $\theta_{pol} = 0°$ as shown in Figs. 3 and 4, in which the x axis in the xyz coordinate system (see the inset of Fig. 3) defined using the E-field direction. Thus, the OR-PAD is defined by both the molecular axis and the laser polarization direction, which means that the OR-PAD has a mixed character of an MF-PAD and a laboratory-frame (LF) PAD. The detailed descriptions of the OR-PAD represented in this xyz coordinate system will be given in Appendix A.

As shown in Fig. 3, the OR-PADs are obtained at the nine different θ_{pol} values with an interval of 10° with the integration range of E_{elec} = 0.8–1.2 eV, corresponding to the energy range of the four-photon ionization to the $\tilde{X}$ state of CH_3OH^+. At $\theta_{pol} = 5°$, the photoelectrons are emitted in the direction almost parallel to the E field as shown in Fig. 3(a). It is also found that the yield of the photoelectrons emitted towards the direction of p_{ion} is slightly larger than that emitted towards the opposite direction of p_{ion}, that is, the yield of electrons emitted in the direction from the O atom to the C atom is slightly larger than the yield of electrons emitted in the direction from the C atom to the O atom. As θ_{pol} increases up to $\theta_{pol} = 85°$, the direction of the photoelectron emission follows the rotation of the E field in the molecular frame so that it is kept to be almost parallel to the E-field direction as shown in Figs. 3(a)–3(i). Thus, in the four-photon ionization to the $\tilde{X}$ state, it can be concluded that the photoelectrons are predominantly emitted along the direction parallel to the E field, irrespective of the direction of p_{ion} in the laboratory frame, that is, the direction of the C-O bond axis.

Figure 4 shows the OR-PADs obtained by the integration over the photoelectron energy range of E_{elec} = 0.2–0.6 eV, corresponding to the energy range of the five-photon ionization to the $\tilde{B}$ state of methanol cation. At $\theta_{pol} = 5°$, the photoelectrons are predominantly emitted in the direction almost parallel to the E field. Contrary to the corresponding case in Fig. 3, the photoelectrons are emitted towards the opposite direction from p_{ion}, that is, the photoelectrons are ejected in the direction from the C atom to the O atom more preferentially than in the direction from the O atom to the C atom as shown in Fig. 4(a). As θ_{pol} increases up to $\theta_{pol} = 85°$, the relative yield of the photoelectrons emitted in the direction
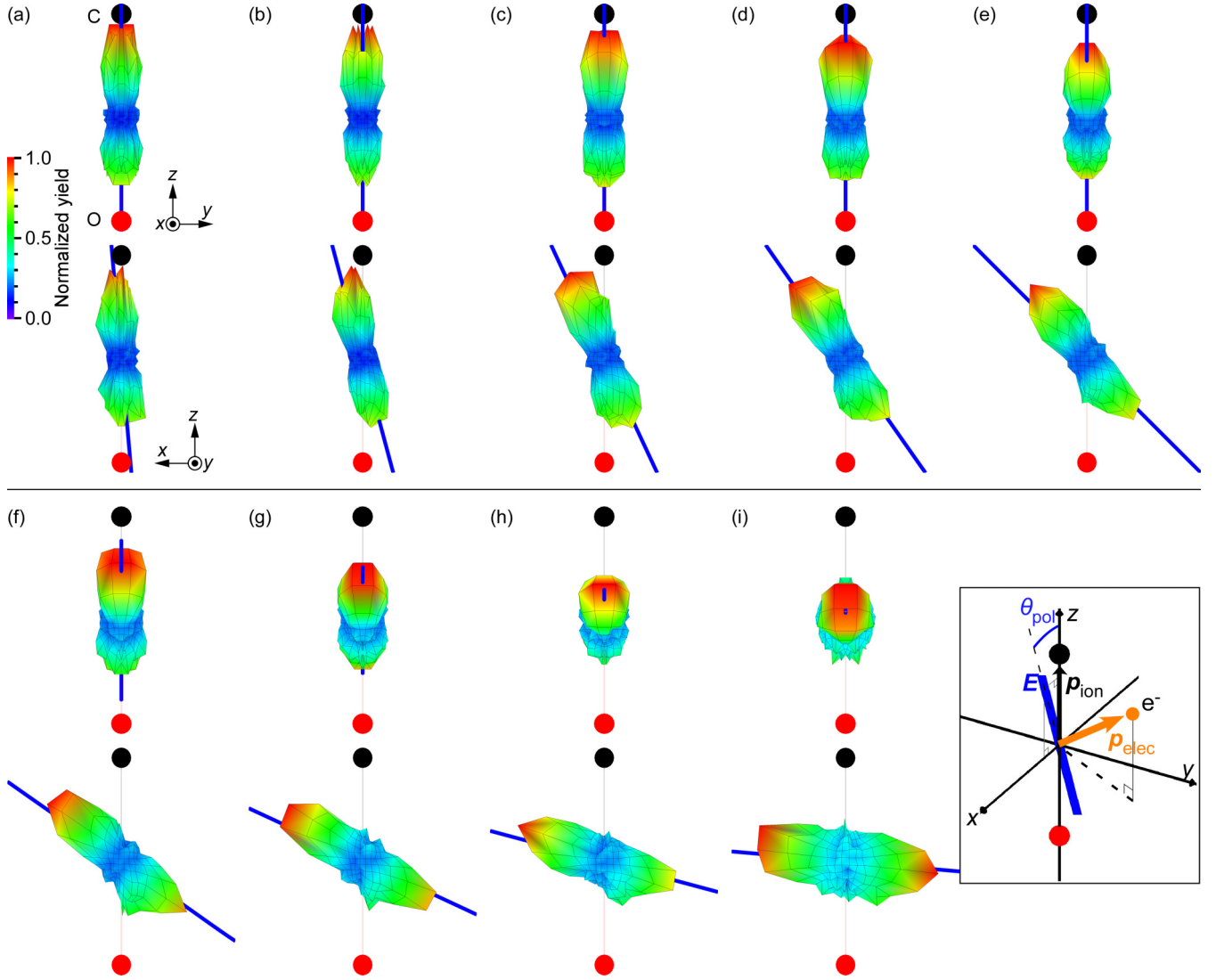
FIG. 3. Stereographic drawing of OR-PADs experimentally derived at $\theta_{\mathrm{pol}} =$ (a) $5°$, (b) $15°$, (c) $25°$, (d) $35°$, (e) $45°$, (f) $55°$, (g) $65°$, (h) $75°$, and (i) $85°$ for the photoelectron energy in the range between 0.8 and 1.2 eV, which is assigned to the four-photon ionization to $\tilde{X}$. The angle between the recoil vector of CH_3^+ $\boldsymbol{p}_{\mathrm{ion}}$, and the laser $\boldsymbol{E}$ field is denoted by θ_{pol}. The yields are normalized by their maxima. The bin size of θ_{pol} is $10°$. Top: View from the positive x axis. Bottom: View from the positive y axis. Blue thick lines indicate the laser polarization directions. Black and red circles are C and O atoms, respectively, and H atoms are omitted. The inset shows the xyz coordinate system and the definition of θ_{pol}. The z axis is along $\boldsymbol{p}_{\mathrm{ion}}$, and the $\boldsymbol{E}$ field lies on the zx plane.

perpendicular to the $\boldsymbol{E}$ field becomes comparable to that in the direction parallel to the $\boldsymbol{E}$ field as shown in Figs. 4(a)–4(i). Because of this perpendicular component, the OR-PADs exhibit a shape of a deformed elliptic disk. At $\theta_{\mathrm{pol}} = 85°$, the elliptic disk on the yz plane is slightly elongated along the y axis, which is perpendicular to the direction of $\boldsymbol{p}_{\mathrm{ion}}$ (the z axis) and to the $\boldsymbol{E}$ field (the x axis). This perpendicular component along the major axis of the ellipse appears as the peak at $\theta_{\mathrm{elec}} = 90°$ in the orientation-angle integrated MF-PAD at $E_{\mathrm{elec}} \sim 0.45$ eV shown in Fig. 1. Thus, in the five-photon ionization to the $\tilde{B}$ state, the yield of the photoelectron emission along the direction perpendicular to the $\boldsymbol{E}$ field increases as θ_{pol} increases to $90°$ while the yield of the photoelectron emission along the $\boldsymbol{E}$ field does not exhibit sensitive dependence on θ_{pol}.

C. Spherical harmonic expansion of OR-PAD

For quantitative discussion, we expand the OR-PADs by the spherical harmonics $Y_{LM}(\theta_{\mathrm{elec}}^{\mathrm{LF}}, \varphi_{\mathrm{elec}}^{\mathrm{LF}})$ as

$$I^{\mathrm{LF}}(\theta_{\mathrm{elec}}^{\mathrm{LF}}, \varphi_{\mathrm{elec}}^{\mathrm{LF}}; \theta_{\mathrm{pol}}) = \frac{1}{\sqrt{4\pi}} C_0(\theta_{\mathrm{pol}}) \sum_{L=0}^{L_{\max}} \sum_{M=-L}^{L} \beta_{LM}(\theta_{\mathrm{pol}})$$
$$\times Y_{LM}(\theta_{\mathrm{elec}}^{\mathrm{LF}}, \varphi_{\mathrm{elec}}^{\mathrm{LF}}), \tag{1}$$

with the expansion coefficients $\beta_{LM}(\theta_{\mathrm{pol}})$, where $\theta_{\mathrm{elec}}^{\mathrm{LF}}$ and $\varphi_{\mathrm{elec}}^{\mathrm{LF}}$ are the polar and azimuthal angles of $\boldsymbol{p}_{\mathrm{elec}}$, respectively, in the orientation-angle-resolved laboratory frame (OR-LF) as shown in Fig. 5. In the OR-PAD, $I^{\mathrm{LF}}(\theta_{\mathrm{elec}}^{\mathrm{LF}}, \varphi_{\mathrm{elec}}^{\mathrm{LF}}; \theta_{\mathrm{pol}})$, $\beta_{00}(\theta_{\mathrm{pol}})$ $(L = M = 0)$ is set to be 1 and $C_0(\theta_{\mathrm{pol}})$ represents the total yield integrated over the
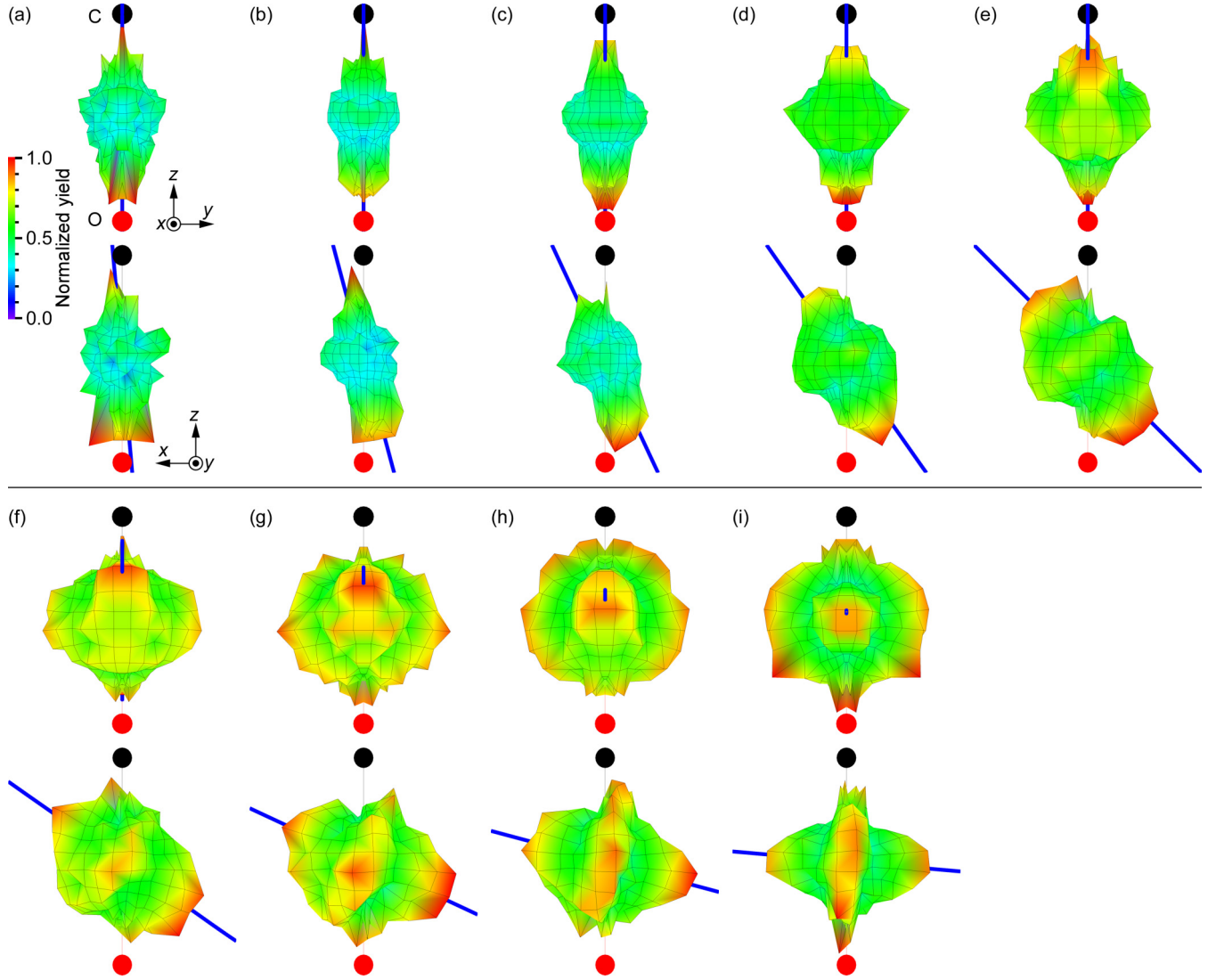
FIG. 4. Stereographic drawing of OR-PADs experimentally derived at $\theta_{\mathrm{pol}} =$ (a) $5°$, (b) $15°$, (c) $25°$, (d) $35°$, (e) $45°$, (f) $55°$, (g) $65°$, (h) $75°$, and (i) $85°$ for the photoelectron energy in the range between 0.2 and 0.6 eV, which is assigned to the five-photon ionization to $\tilde{B}$. The yields are normalized by their maxima. The bin size of θ_{pol} is $10°$. Top: View from the positive x axis. Bottom: View from the positive y axis. Blue thick lines indicate the laser polarization directions. Black and red circles are C and O atoms, respectively, and H atoms are omitted.

entire ranges of $\theta_{\mathrm{elec}}^{\mathrm{LF}}$ and $\varphi_{\mathrm{elec}}^{\mathrm{LF}}$, which can be given using the alignment-angle dependent ionization probability, $W(\theta_{\mathrm{pol}})$, as

$$C_0(\theta_{\mathrm{pol}}) = W(\theta_{\mathrm{pol}}) \sin\theta_{\mathrm{pol}}. \tag{2}$$

As seen in Fig. 5, the Z' axis of the $X'Y'Z'$ coordinate system is set to be along the $\boldsymbol{E}$-field direction. From the condition

that $I^{\mathrm{LF}}(\theta_{\mathrm{elec}}^{\mathrm{LF}}, \varphi_{\mathrm{elec}}^{\mathrm{LF}}; \theta_{\mathrm{pol}})$ is real and is symmetric with respect to the $Z'X'$ plane shown in Fig. 5, $\beta_{LM}(\theta_{\mathrm{pol}})$ must be real and satisfy the following relation:

$$\beta_{L-M}(\theta_{\mathrm{pol}}) = (-1)^M \beta_{LM}(\theta_{\mathrm{pol}}). \tag{3}$$

Therefore, Eq. (1) is rewritten using $\beta_{LM}(\theta_{\mathrm{pol}})$ with $M \geqslant 0$ as

$$
\begin{aligned}
& I^{\mathrm{LF}}\big(\theta_{\mathrm{elec}}^{\mathrm{LF}}, \varphi_{\mathrm{elec}}^{\mathrm{LF}}; \theta_{\mathrm{pol}}\big) \\
& = \frac{1}{\sqrt{4\pi}} C_0(\theta_{\mathrm{pol}}) \left\{ \sum_{L=0}^{L_{\max}} \beta_{L0}(\theta_{\mathrm{pol}}) Y_{L0}\big(\theta_{\mathrm{elec}}^{\mathrm{LF}}, \varphi_{\mathrm{elec}}^{\mathrm{LF}}\big) + \sum_{L=1}^{L_{\max}} \sum_{M=1}^{L} \beta_{LM}(\theta_{\mathrm{pol}}) \big[Y_{LM}\big(\theta_{\mathrm{elec}}^{\mathrm{LF}}, \varphi_{\mathrm{elec}}^{\mathrm{LF}}\big) + (-1)^M Y_{L-M}\big(\theta_{\mathrm{elec}}^{\mathrm{LF}}, \varphi_{\mathrm{elec}}^{\mathrm{LF}}\big) \big] \right\} \\
& = \frac{1}{\sqrt{4\pi}} C_0(\theta_{\mathrm{pol}}) \left\{ \sum_{L=0}^{L_{\max}} \beta_{L0}(\theta_{\mathrm{pol}}) Y_{L0}\big(\theta_{\mathrm{elec}}^{\mathrm{LF}}, \varphi_{\mathrm{elec}}^{\mathrm{LF}}\big) + 2 \sum_{L=1}^{L_{\max}} \sum_{M=1}^{L} \beta_{LM}(\theta_{\mathrm{pol}}) \mathrm{Re}\big[Y_{LM}\big(\theta_{\mathrm{elec}}^{\mathrm{LF}}, \varphi_{\mathrm{elec}}^{\mathrm{LF}}\big) \big] \right\}. \tag{4}
\end{aligned}
$$
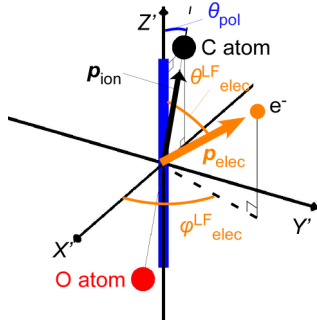
FIG. 5. Definitions of $\theta_{\text{elec}}^{\text{LF}}$, $\varphi_{\text{elec}}^{\text{LF}}$, and θ_{pol} in the OR-LF with the $X'Y'Z'$ coordinates. The Z' axis is set to be along the $\boldsymbol{E}$-field direction. The CH_3^+ recoil vector $\boldsymbol{p}_{\text{ion}}$ lies on the $Z'X'$ plane and the directions of Z' and X' axes are defined so that the Z' and X' components of $\boldsymbol{p}_{\text{ion}}$ are positive and negative, respectively.

The expansion coefficients $\beta_{LM}(\theta_{\text{pol}})$ are obtained from the OR-PADs by the procedure to be given in Appendix B. Figures 6 and 7 show the coefficients, $\beta_{LM}(\theta_{\text{pol}})(1 \leqslant L \leqslant 4,\ 0 \leqslant M \leqslant L)$, for the four-photon ionization to the $\tilde{X}$ state and the five-photon ionization to the $\tilde{B}$ state, respectively. Using these coefficients, $\beta_{LM}(\theta_{\text{pol}})$, of the OR-PAD, the photoelectron emission dynamics is discussed in the following subsections.

D. Photoelectron emission parallel to the laser E field

As shown in the OR-PADs in Figs. 3 and 4, the photoelectrons tend to be emitted in the direction parallel to the $\boldsymbol{E}$ field ($\theta_{\text{elec}}^{\text{LF}} = 0°$ and $180°$) as well as in the direction perpendicular to the $\boldsymbol{E}$ field ($\theta_{\text{elec}}^{\text{LF}} = 90°$). In this subsection, we examine how the photoelectron emission in the direction parallel to the $\boldsymbol{E}$ field varies as a function of the molecular orientation angle θ_{pol}. The tendency of the parallel emission is represented by $\beta_{20}(\theta_{\text{pol}})$ and $\beta_{40}(\theta_{\text{pol}})$, both of which are positive and whose
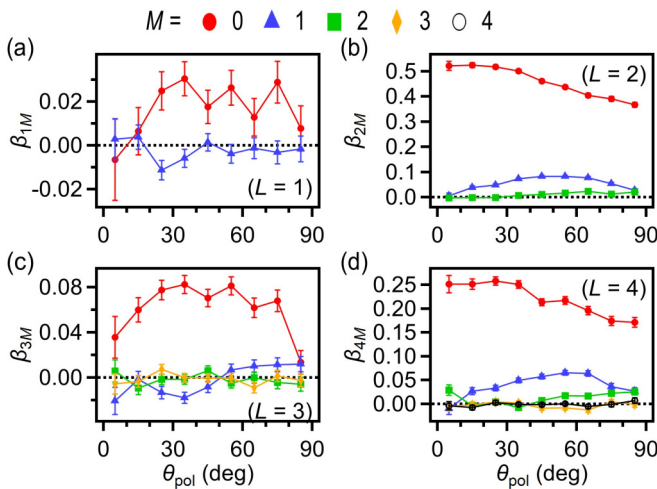
FIG. 6. Expansion coefficients $\beta_{LM}(\theta_{\text{pol}})$ [$L = 1$ (a), 2 (b), 3 (c), and 4 (d)] as a function of θ_{pol} for $E_{\text{elec}} = 0.8–1.2$ eV, which is assigned to the four-photon ionization to $\tilde{X}$. Red solid circles, blue triangles, green squares, yellow diamonds, and black open circles represent $M = 0$, 1, 2, 3, and 4, respectively.
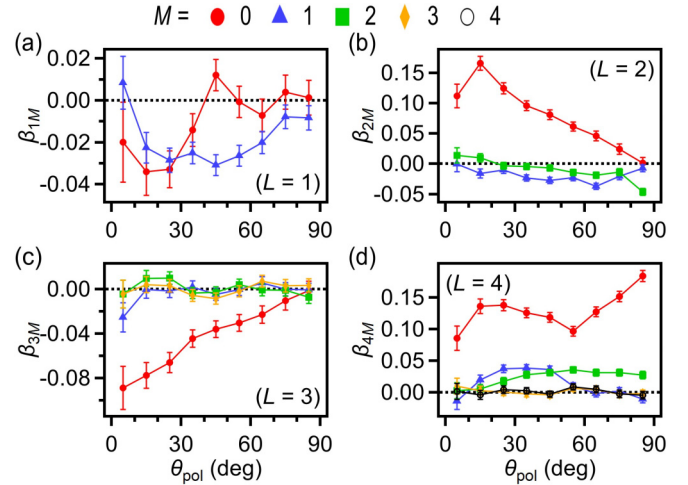
FIG. 7. Expansion coefficients $\beta_{LM}(\theta_{\text{pol}})$ [$L = 1$ (a), 2 (b), 3 (c), and 4 (d)] as a function of θ_{pol} for the photoelectron energy in the range between 0.2 and 0.6 eV, which is assigned to the five-photon ionization to $\tilde{B}$. Red solid circles, blue triangles, green squares, yellow diamonds, and black open circles represent $M = 0$, 1, 2, 3, and 4, respectively.

absolute values are much larger than the other $\beta_{LM}(\theta_{\text{pol}})$ coefficients as shown in Figs. 6 and 7.

We discuss the influence of the spatial distribution of the canonical molecular orbitals, from which a photoelectron is emitted. The molecular orbitals in the ground state of methanol are calculated by employing density-functional theory with the exchange-correlation functional of the Krieger-Li-Iafrate self-interaction correlation [20]. The ionization to the $\tilde{X}$ and $\tilde{B}$ states is considered to take place through the photoelectron emission from the $2a''$ and $6a'$ molecular orbitals, respectively. The electronic configuration of the ground state of neutral methanol, CH_3OH, is ... $(5a')^2(1a'')^2(6a')^2(7a')^2(2a'')^2$. As shown in Fig. 8(a), the $2a''$ molecular orbital, from which an electron is emitted in the ionization to the $\tilde{X}$ state, has a nodal plane almost perpendicular to the C-O bond. Therefore, when the $\boldsymbol{E}$ field is perpendicular to the C-O axis ($\theta_{\text{pol}} = 90°$), the $\boldsymbol{E}$ field is in the direction parallel to the nodal plane, resulting in the suppression of the probability of the photoelectron emission at $\theta_{\text{pol}} = 90°$ by destructive interference between the photoelectron emission from the two lobes of $2a''$ having the opposite phases [21,22].

Similarly the ionization probability at around $\theta_{\text{pol}} = 0°$ is expected to be suppressed by the destructive interference in the photoelectron emission because the $2a''$ molecular orbital has another nodal plane containing the C-O axis in addition to the nodal plane perpendicular to the C-O axis as shown in Fig. 8(a). However, as shown in Fig. 9(a), the alignment-angle dependent ionization probability $W(\theta_{\text{pol}})$ obtained from the angular distribution of the CH_3^+ recoil measured in coincidence with photoelectrons in the energy range of 0.8–1.2 eV exhibits a peak at $\theta_{\text{pol}} = 0°$, showing that CH_3^+ is predominantly ejected in the direction along to the $\boldsymbol{E}$ field. This seemingly contradicting situation at $\theta_{\text{pol}} = 0°$ can be ascribed to dynamical molecular alignment [23], in which the
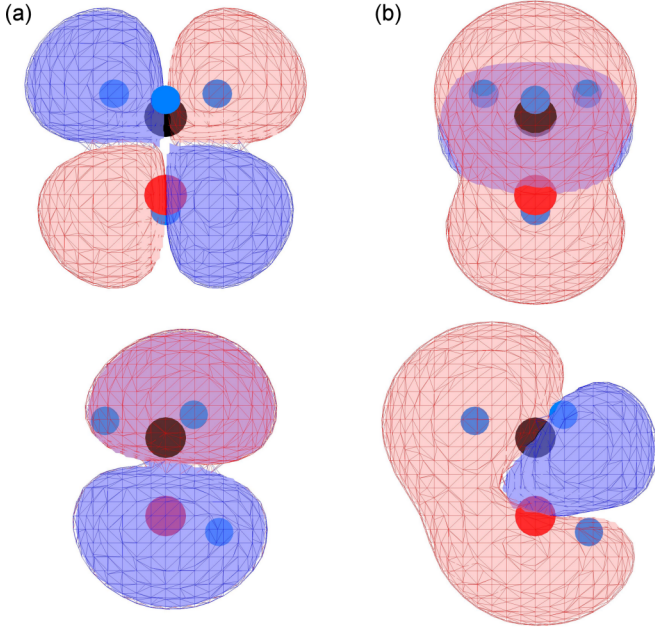
FIG. 8. Isosurface plots at 0.01 au [red (light gray)] and -0.01 au [blue (dark gray)] of the molecular orbitals (a) $2a''$ and (b) $6a'$ viewed from two different angles.

molecular axis is aligned towards the $\boldsymbol{E}$ field in the course of the dissociation after the photoelectron emission [24]. Therefore, the polarization angle θ_{pol} can be decreased from the initial angle at the moment of the photoelectron emission to the final angle recorded as the recoil direction of the CH_3^+ fragment ion. It was reported that the effect of the dynamical alignment can be significantly suppressed by shortening the pulse duration to be as short as 7 fs [23]. Indeed, the measured angular distribution of the fragment ions exhibits a four-leaf shape reflecting the shape of the $2a''$ HOMO. Therefore, we can assume that the angular distribution of the molecular axis is hardly blurred by the dynamical alignment in the 7-fs pulse. The averaged recoil angle of CH_3^+ with respect to the laser
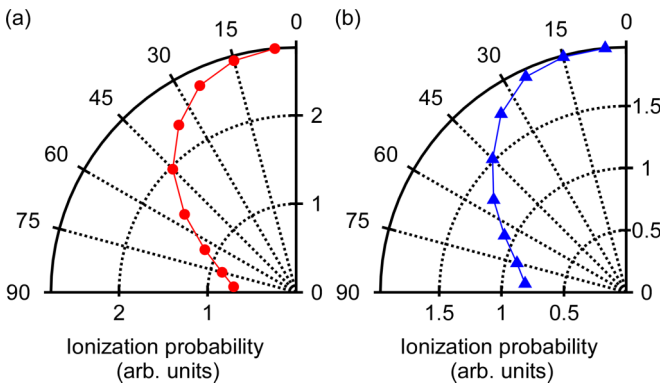
FIG. 9. Alignment-angle dependent ionization probability $W(\theta_{\mathrm{pol}})$ experimentally measured as a function of θ_{pol} for (a) $E_{\mathrm{elec}} = 0.8$–1.2 eV (the four-photon ionization to $\tilde{X}$) and (b) $E_{\mathrm{elec}} = 0.2$–0.6 eV (the five-photon ionization to $\tilde{B}$). Each plot is the cross section of the 3D probability distribution, which is cylindrically symmetric with respect to the $\boldsymbol{E}$ field.

polarization direction is 34.5° in the present study while that obtained using the 7-fs pulse is 39.1° [23]. This difference of $4.6°(=39.1°-34.5°)$ in the recoil angle can be regarded as a rough estimate of the extent of the dynamical alignment in the present study. For the four-photon ionization to the $\tilde{X}$ state, the orientation-angle dependent probability of the electronic excitation to the higher-lying electronic states above the dissociation energy threshold can also be included in $W(\theta_{\mathrm{pol}})$.

In the course of the accumulation of the ionization events for construction of OR-PADs, the bin size of θ_{pol} is set to be $10°$, which is larger than the extent of the dynamical alignment discussed above. Therefore, the OR-PADs obtained in the present study as a function of θ_{pol} contain the uncertainty of around $10°$ in the direction of the molecular orientation, which can be regarded also as the angular resolution in the present experiment.

As seen in Figs. 3 and 4, the photoelectron emission in the direction parallel to the $\boldsymbol{E}$ field exhibits asymmetry, that is, the yield of the photoelectron emission towards the positive Z' direction, corresponding to the electron emission in the same direction as $\boldsymbol{p}_{\mathrm{ion}}$ and the yield of the photoelectron emission towards the negative Z' direction, corresponding to the photoelectron emission in the direction opposite to $\boldsymbol{p}_{\mathrm{ion}}$ are different to a certain extent. We define the asymmetry parameter $P_{\mathrm{asym}}(\theta_{\mathrm{pol}})$ whose value is in the range of $-1 \leqslant P_{\mathrm{asym}}(\theta_{\mathrm{pol}}) \leqslant 1$ as

$$P_{\mathrm{asym}}(\theta_{\mathrm{pol}}) = \frac{S_{\mathrm{C}}^{\mathrm{LF}}(\theta_{\mathrm{pol}}) - S_{\mathrm{O}}^{\mathrm{LF}}(\theta_{\mathrm{pol}})}{S_{\mathrm{C}}^{\mathrm{LF}}(\theta_{\mathrm{pol}}) + S_{\mathrm{O}}^{\mathrm{LF}}(\theta_{\mathrm{pol}})}, \quad (5)$$

where

$$S_{\mathrm{C}}^{\mathrm{LF}}(\theta_{\mathrm{pol}})$$
$$= \int_{-\pi}^{\pi} \left[\int_{0}^{\Delta\theta} I^{\mathrm{LF}}(\theta_{\mathrm{elec}}^{\mathrm{LF}}, \varphi_{\mathrm{elec}}^{\mathrm{LF}}; \theta_{\mathrm{pol}}) \sin\theta_{\mathrm{elec}}^{\mathrm{LF}} \, d\theta_{\mathrm{elec}}^{\mathrm{LF}} \right] d\varphi_{\mathrm{elec}}^{\mathrm{LF}}$$
$$(6)$$

and

$$S_{\mathrm{O}}^{\mathrm{LF}}(\theta_{\mathrm{pol}})$$
$$= \int_{-\pi}^{\pi} \left[\int_{\pi-\Delta\theta}^{\pi} I^{\mathrm{LF}}(\theta_{\mathrm{elec}}^{\mathrm{LF}}, \varphi_{\mathrm{elec}}^{\mathrm{LF}}; \theta_{\mathrm{pol}}) \sin\theta_{\mathrm{elec}}^{\mathrm{LF}} \, d\theta_{\mathrm{elec}}^{\mathrm{LF}} \right] d\varphi_{\mathrm{elec}}^{\mathrm{LF}},$$
$$(7)$$

representing the yield of the photoelectron emission in the same direction as $\boldsymbol{p}_{\mathrm{ion}}$ and that in the direction opposite to $\boldsymbol{p}_{\mathrm{ion}}$, respectively. As the polar angle range $\Delta\theta$ in the integration in Eqs. (6) and (7), we adopt $\Delta\theta = 30°$ as shown in Fig. 10(a). Note that the maximum and minimum values of $P_{\mathrm{asym}}(\theta_{\mathrm{pol}})$, that is, $P_{\mathrm{asym}}(\theta_{\mathrm{pol}}) = +1$ and -1, mean, respectively, that the photoelectrons are emitted exclusively in the same direction as $\boldsymbol{p}_{\mathrm{ion}}$ and in the direction opposite to $\boldsymbol{p}_{\mathrm{ion}}$. At $\theta_{\mathrm{pol}} = 90°$, the asymmetry parameter becomes $P_{\mathrm{asym}}(\theta_{\mathrm{pol}}) = 0$ because the photoelectron emission exhibits reflection symmetry with respect to the $X'Y'$ plane in Fig. 10(a) at $\theta_{\mathrm{pol}} = 90°$.

Figure 10(b) shows $P_{\mathrm{asym}}(\theta_{\mathrm{pol}})$ in the two photoelectron kinetic energy regions. For the four-photon ionization to the $\tilde{X}$ state ($E_{\mathrm{elec}} = 0.8$–1.2 eV), $P_{\mathrm{asym}}(\theta_{\mathrm{pol}})$ is positive in the entire θ_{pol} range and takes the value of $P_{\mathrm{asym}}(\theta_{\mathrm{pol}}) \sim 0.1$ in the range of $\theta_{\mathrm{pol}} = 25°$–$75°$, indicating that the yield of the photoelectron emission in the same direction as $\boldsymbol{p}_{\mathrm{ion}}$ is larger than
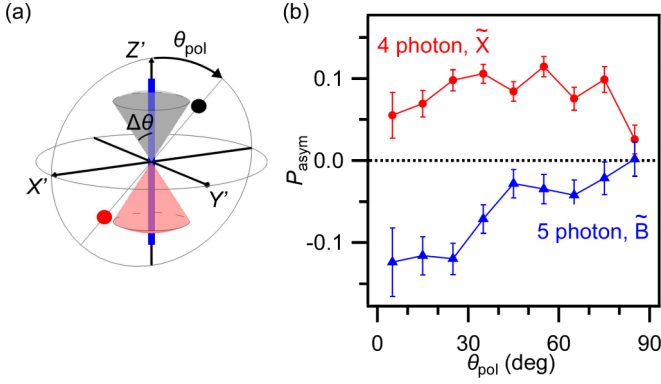
FIG. 10. (a) Definition of the angular range $\Delta\theta$ in the integration for $S_C^{\text{LF}}(\theta_{\text{pol}})$ (gray shaded range) and $S_O^{\text{LF}}(\theta_{\text{pol}})$ (red shaded range). We adopt $\Delta\theta = 30°$. (b) The asymmetry parameters defined in Eq. (5) as a function of θ_{pol}. The red circles are for $E_{\text{elec}} = 0.8$–1.2 eV (the four-photon ionization to $\tilde{X}$) and the blue triangles are for $E_{\text{elec}} = 0.2$–0.6 eV (the five-photon ionization to $\tilde{B}$).

that in the direction opposite to $\boldsymbol{p}_{\text{ion}}$. On the other hand, for the five-photon ionization to the $\tilde{B}$ state ($E_{\text{elec}} = 0.2$–0.8 eV), $P_{\text{asym}}(\theta_{\text{pol}})$ is negative in the range of $\theta_{\text{pol}} = 5°$–$75°$, indicating that the yield of the photoelectron emission in the direction opposite to $\boldsymbol{p}_{\text{ion}}$ is larger than that in the same direction as $\boldsymbol{p}_{\text{ion}}$. When $\theta_{\text{pol}} = 0°$–$25°$, $P_{\text{asym}}(\theta_{\text{pol}})$ exhibits relatively large negative values of around -0.12, and as θ_{pol} increases from $\theta_{\text{pol}} = 25°$ to $45°$, the absolute value decreases so that $P_{\text{asym}}(\theta_{\text{pol}})$ becomes around -0.04 at $\theta_{\text{pol}} = 45°$.

The asymmetry of the OR-PAD is described by the expansion coefficients such as β_{10} and β_{30} in Eq. (1) for the spherical harmonics having odd symmetry with respect to the inversion at their origins. When $\beta_{10}(\theta_{\text{pol}})$ and $\beta_{30}(\theta_{\text{pol}})$ are positive, the probability of the photoelectron emission in the same direction as $\boldsymbol{p}_{\text{ion}}$ is more enhanced than that in the direction opposite to $\boldsymbol{p}_{\text{ion}}$. On the other hand, when $\beta_{10}(\theta_{\text{pol}})$ and $\beta_{30}(\theta_{\text{pol}})$ are negative, the probability of the photoelectron emission in the direction opposite to $\boldsymbol{p}_{\text{ion}}$ is more enhanced than that in the same direction as $\boldsymbol{p}_{\text{ion}}$. As shown in Figs. 6(a) and 6(c), for the four-photon ionization to the $\tilde{X}$ state, both $\beta_{10}(\theta_{\text{pol}})$ and $\beta_{30}(\theta_{\text{pol}})$ are positive in the range of $\theta_{\text{pol}} = 15°$–$75°$, representing that the yield of the photoelectron emission in the same direction as $\boldsymbol{p}_{\text{ion}}$ is more enhanced than in the direction opposite to $\boldsymbol{p}_{\text{ion}}$.

For the five-photon ionization to the $\tilde{B}$ state, it is found that $\beta_{30}(\theta_{\text{pol}})$ is negative in the entire θ_{pol} range, representing that the probability of the photoelectron emission in the direction opposite to $\boldsymbol{p}_{\text{ion}}$ is more enhanced than that in the same direction as $\boldsymbol{p}_{\text{ion}}$ and its absolute value decreases monotonically as θ_{pol} increases. On the other hand, $\beta_{10}(\theta_{\text{pol}})$ takes negative values in the range of $\theta_{\text{pol}} = 5°$–$35°$ and becomes almost zero in the range of $\theta_{\text{pol}} = 55°$–$85°$, leading to the suppression of the asymmetry as shown in Fig. 10(b).

As shown in Fig. 3, the recorded OR-PADs shows that the direction of the photoelectron emission is slightly deflected from the direction of the $\boldsymbol{E}$ field. In order to evaluate quantitatively the extent of the deviation of the direction of the photoelectron emission from the direction of the $\boldsymbol{E}$ field, we accumulate the yield of the photoelectrons emitted in the
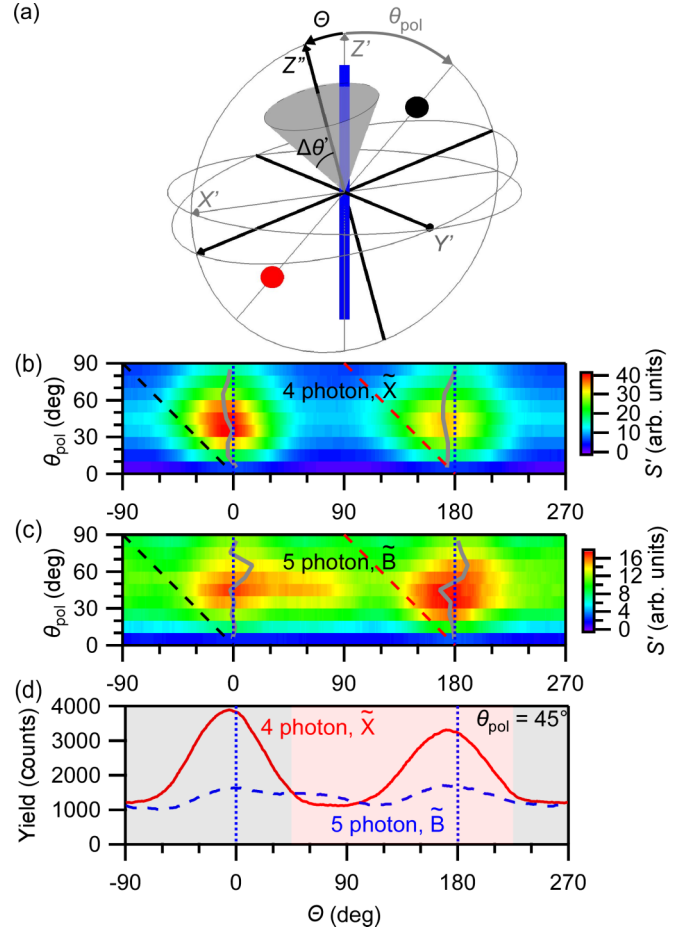
FIG. 11. (a) Definition of the Z'' axis, which is on the Z'-X' plane and deflected from the Z' axis by the deflection angle Θ, and the angular range $\Delta\theta'$ in the integration for $S'(\Theta; \theta_{\text{pol}})$. We adopt $\Delta\theta' = 30°$. (b) and (c) 2D maps of $S'(\Theta; \theta_{\text{pol}})$ for $E_{\text{elec}} = 0.8$–1.2 eV (the four-photon ionization to $\tilde{X}$) (b) and for $E_{\text{elec}} = 0.2$–0.6 eV (the five-photon ionization to $\tilde{B}$) (c). (d) The cross section of the 2D maps in (b) (red solid line) and (c) (blue dashed line) at $\theta_{\text{pol}} = 45°$. In (b) and (c), the blue dotted lines represent the direction of the $\boldsymbol{E}$ field, the black and red dashed lines represent the directions along the C-O bond axis towards the C and O atom sides, respectively, and the gray solid lines represent the Θ value at which $S'(\Theta; \theta_{\text{pol}})$ becomes maximum in the range of $\Theta = -90°$–$90°$ and that in the range of $\Theta = 90°$–$270°$. In (b) the photoelectrons are emitted dominantly in the direction parallel to the $\boldsymbol{E}$ field ($\Theta = 0°$ and $180°$), but slightly shifted by $5°$–$10°$ toward the C-O bond axis from the $\boldsymbol{E}$-field direction. In (d) the blue dotted lines represent the direction of the $\boldsymbol{E}$ field, and the gray and red shaded areas correspond to the photoelectron emission in the same direction as $\boldsymbol{p}_{\text{ion}}$ and that in the direction opposite to $\boldsymbol{p}_{\text{ion}}$, respectively. The angle Θ ranges from $-89.5°$ to $269.5°$ with the $1°$ step.

direction centered about the Z'' axis, which is on the Z'-X' plane and deflected from the Z' axis by the deflection angle Θ, as shown in Fig. 11(a). The yield of photoelectrons emitted within the angle range of $0° \leqslant \theta'_{\text{elec}} \leqslant \Delta\theta'$, where θ'_{elec} is the angle of the direction of the photoelectron emission with respect to the Z'' axis, is accumulated as $S'(\Theta; \theta_{\text{pol}})$. The upper bound of the angle θ'_{elec} is set to be $\Delta\theta' = 30°$. As can be seen in Fig. 11, when a photoelectron is emitted in
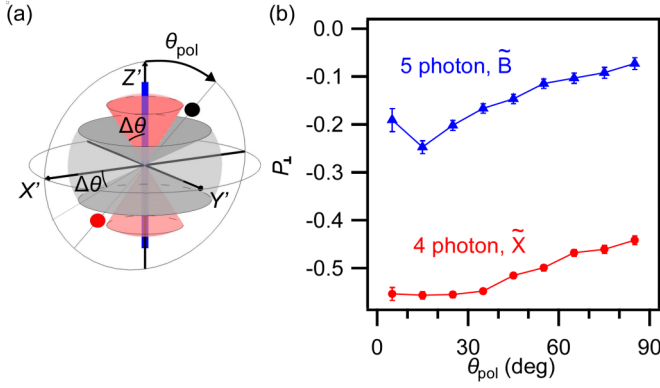
FIG. 12. (a) Definition of the angular range $\Delta\theta$ in the integration for $S_\perp^{\mathrm{LF}}(\theta_{\mathrm{pol}})$ (gray shaded range) and $S_{||}^{\mathrm{LF}}(\theta_{\mathrm{pol}})$ (red shaded range). We adopt $\Delta\theta = 30°$. (b) The perpendicular emission parameters defined in Eq. (8) as a function of θ_{pol}. The red circles are for $E_{\mathrm{elec}} = 0.8$–1.2 eV (the four-photon ionization to $\tilde{X}$) and the blue triangles are for $E_{\mathrm{elec}} = 0.2$–0.6 eV (the five-photon ionization to $\tilde{B}$).

the direction from the O atom to the C atom, $S'(\Theta; \theta_{\mathrm{pol}})$ at $\Theta = -\theta_{\mathrm{pol}}$ becomes large while, when a photoelectron is emitted in the direction from the C atom to the O atom, $S'(\Theta; \theta_{\mathrm{pol}})$ at $\Theta = (180° - \theta_{\mathrm{pol}})$ becomes large.

In Fig. 11(b), the accumulated yield, $S'(\Theta; \theta_{\mathrm{pol}})$ for the four-photon ionization to the $\tilde{X}$ state of $\mathrm{CH_3OH^+}$ is plotted. It can be said that the yield takes two maxima at around $(\Theta, \theta_{\mathrm{pol}}) = (0°, 45°)$ and $(180°, 45°)$, but, if we take a closer look, at $\theta_{\mathrm{pol}} = 45°$, the maximum yield is found to be achieved at $\Theta = -5.5°$ and $170.5°$ as shown in Fig. 11(d), which means that the ejection direction of a photoelectron is deflected from the laser polarization direction towards the C-O bond axis by $5.5°$ and $9.5°$, respectively. We confirm that these deflection angles do not sensitively depend on $\Delta\theta'$. Indeed, even when

$\Delta\theta'$ is increased from $30°$ to $45°$, the deflection angle of $5.5°$ is increased only by $3°$ to $8.5°$ and the deflection angle of $9.5°$ is increased only by $4°$ to $13.5°$.

As shown in Figs. 6(b) and 6(d), both $\beta_{21}(\theta_{\mathrm{pol}})$ and $\beta_{41}(\theta_{\mathrm{pol}})$ exhibit significant positive deviations from zero in the range of $\theta_{\mathrm{pol}} = 15°$–$85°$, reflecting the fact that the OR-PAD is distorted from cylindrical symmetry with respect to the $\boldsymbol{E}$ field, so that the direction of the photoelectron emission is deflected towards the direction of the C-O bond axis by $5°$–$10°$ from the laser polarization direction as explained above. This deviation from the $\boldsymbol{E}$-field direction can be ascribed to the anisotropic Coulomb potential [25–28] within $\mathrm{CH_3OH}$ acting on the escaping photoelectron.

In Fig. 11(c), the accumulated yield, $S'(\Theta; \theta_{\mathrm{pol}})$ for the five-photon ionization to the $\tilde{B}$ state of $\mathrm{CH_3OH^+}$ is plotted. In a similar manner as in Fig. 11(b), the yield exhibit two maxima at around $(\Theta, \theta_{\mathrm{pol}}) = (0°, 45°)$ and $(180°, 45°)$. A flat part of the distribution in the range from $\Theta = 0°$ to $90°$ around $\theta_{\mathrm{pol}} = 45°$ corresponds to the photoelectron emission along the direction perpendicular to the $\boldsymbol{E}$ field as shown in Fig. 4.

E. Photoelectron emission perpendicular to laser $\boldsymbol{E}$ field

In this subsection, we examine how the photoelectron emission in the direction perpendicular to the $\boldsymbol{E}$ field varies as a function of the molecular orientation angle θ_{pol}. The extent of the photoelectron emission in the direction perpendicular to the $\boldsymbol{E}$ field can be represented by $P_\perp(\theta_{\mathrm{pol}})$ defined as

$$P_\perp(\theta_{\mathrm{pol}}) = \frac{S_\perp^{\mathrm{LF}}(\theta_{\mathrm{pol}}) - S_{||}^{\mathrm{LF}}(\theta_{\mathrm{pol}})}{S_\perp^{\mathrm{LF}}(\theta_{\mathrm{pol}}) + S_{||}^{\mathrm{LF}}(\theta_{\mathrm{pol}})}, \qquad (8)$$

where $S_{||}^{\mathrm{LF}}(\theta_{\mathrm{pol}})$ and $S_\perp^{\mathrm{LF}}(\theta_{\mathrm{pol}})$ represent the yields of the photoelectrons emitted in the directions parallel and perpendicular to the $\boldsymbol{E}$ field per unit solid angle, respectively, and are given by

$$S_{||}^{\mathrm{LF}}(\theta_{\mathrm{pol}}) = \frac{\int_{-\pi}^{\pi} \left[\int_0^{\Delta\theta} I^{\mathrm{LF}}(\theta_{\mathrm{elec}}^{\mathrm{LF}}, \varphi_{\mathrm{elec}}^{\mathrm{LF}}; \theta_{\mathrm{pol}}) \sin\theta_{\mathrm{elec}}^{\mathrm{LF}} d\theta_{\mathrm{elec}}^{\mathrm{LF}} + \int_{\pi-\Delta\theta}^{\pi} I^{\mathrm{LF}}(\theta_{\mathrm{elec}}^{\mathrm{LF}}, \varphi_{\mathrm{elec}}^{\mathrm{LF}}; \theta_{\mathrm{pol}}) \sin\theta_{\mathrm{elec}}^{\mathrm{LF}} d\theta_{\mathrm{elec}}^{\mathrm{LF}} \right] d\varphi_{\mathrm{elec}}^{\mathrm{LF}}}{2 \int_{-\pi}^{\pi} \left[\int_0^{\Delta\theta} \sin\theta_{\mathrm{elec}}^{\mathrm{LF}} d\theta_{\mathrm{elec}}^{\mathrm{LF}} \right] d\varphi_{\mathrm{elec}}^{\mathrm{LF}}} \qquad (9)$$

and

$$S_\perp^{\mathrm{LF}}(\theta_{\mathrm{pol}}) = \frac{\int_{-\pi}^{\pi} \left[\int_{\frac{\pi}{2}-\Delta\theta}^{\frac{\pi}{2}+\Delta\theta} I^{\mathrm{LF}}(\theta_{\mathrm{elec}}^{\mathrm{LF}}, \varphi_{\mathrm{elec}}^{\mathrm{LF}}; \theta_{\mathrm{pol}}) \sin\theta_{\mathrm{elec}}^{\mathrm{LF}} d\theta_{\mathrm{elec}}^{\mathrm{LF}} \right] d\varphi_{\mathrm{elec}}^{\mathrm{LF}}}{\int_{-\pi}^{\pi} \left[\int_{\frac{\pi}{2}-\Delta\theta}^{\frac{\pi}{2}+\Delta\theta} \sin\theta_{\mathrm{elec}}^{\mathrm{LF}} d\theta_{\mathrm{elec}}^{\mathrm{LF}} \right] d\varphi_{\mathrm{elec}}^{\mathrm{LF}}}. \qquad (10)$$

The angular ranges for the integrals of Eqs. (9) and (10) specified using $\Delta\theta = 30°$ are shown in Fig. 12(a). The quantity, $P_\perp(\theta_{\mathrm{pol}})$, given by Eq. (8) is in the range of $-1 \leqslant P_\perp(\theta_{\mathrm{pol}}) \leqslant 1$ by definition and becomes maximum $[P_\perp(\theta_{\mathrm{pol}}) = 1]$ and minimum $[P_\perp(\theta_{\mathrm{pol}}) = -1]$ when all the photoelectrons are emitted in the direction perpendicular and parallel to the direction of the $\boldsymbol{E}$ field, respectively.

In the case of the four-photon ionization to the $\tilde{X}$ state, as shown in Fig. 12(b), $P_\perp(\theta_{\mathrm{pol}})$ takes almost constant values of around -0.56 in the range of $\theta_{\mathrm{pol}} = 5°$–$25°$ and increases monotonically from -0.56 to -0.44 as θ_{pol} increases from

$25°$ to $85°$. As shown in Figs. 6(b) and 6(d), both $\beta_{20}(\theta_{\mathrm{pol}})$ and $\beta_{40}(\theta_{\mathrm{pol}})$ decrease as θ_{pol} increases from $\theta_{\mathrm{pol}} = 25°$ to $85°$, resulting in the increase in $P_\perp(\theta_{\mathrm{pol}})$ so that the OR-PAD becomes more isotropic. On the other hand, in the case of the five-photon ionization to the $\tilde{B}$ state, the $P_\perp(\theta_{\mathrm{pol}})$ value shown in Fig. 12(b) decreases first as θ_{pol} increases from $5°$, takes the minimum value of -0.25 at $\theta_{\mathrm{pol}} = 15°$, and increases monotonically to -0.07 at $\theta_{\mathrm{pol}} = 85°$. The absolute values of $P_\perp(\theta_{\mathrm{pol}})$ are much smaller than those for the four-photon ionization to the $\tilde{X}$ state. As shown in Figs. 7(b) and 7(d), $\beta_{20}(\theta_{\mathrm{pol}})$ decreases monotonically as θ_{pol} increases from

$\theta_{\text{pol}} = 15°$ to $85°$ while $\beta_{40}(\theta_{\text{pol}})$ increases as θ_{pol} increases from $\theta_{\text{pol}} = 55°$ to $85°$. At $\theta_{\text{pol}} = 85°$, $|\beta_{40}(\theta_{\text{pol}})|$ reaches 0.18 while $|\beta_{20}(\theta_{\text{pol}})|$ becomes almost zero. The $\beta_{40}(\theta_{\text{pol}})$ value represents the magnitude of the $Y_{40}(\theta_{\text{elec}}^{\text{LF}}, \varphi_{\text{elec}}^{\text{LF}})$ component and the positive value indicates that the photoelectron yield increases at around $\theta_{\text{elec}}^{\text{LF}} = 90°$, while it decreases at around $\theta_{\text{elec}}^{\text{LF}} = 49°$, where the Legendre polynomial $P_4(\cos\theta_{\text{elec}}^{\text{LF}})$ takes the minimum value. Therefore, the relatively large positive $\beta_{40}(\theta_{\text{pol}})$ value at around $\theta_{\text{pol}} = 90°$ represents the photoelectron emission in the direction perpendicular to the $\boldsymbol{E}$ field, resulting in the small absolute value of $P_\perp(\theta_{\text{pol}})$. As shown in

Figs. 7(b) and 7(d), $\beta_{22}(\theta_{\text{pol}})$ and $\beta_{42}(\theta_{\text{pol}})$ for the five-photon ionization to the $\tilde{B}$ state at $\theta_{\text{pol}} = 85°$ are negative and positive, respectively. These nonzero values of $\beta_{22}(\theta_{\text{pol}})$ and $\beta_{42}(\theta_{\text{pol}})$ with $M = 2$ indicate that the OR-PAD is not cylindrically symmetric with respect to the $\boldsymbol{E}$ field as represented well by the elliptic-disk-shaped perpendicular component of the OR-PAD shown in Fig. 4(i).

As shown above, the shape of the OR-PAD described in Eq. (1) can be discussed based on the obtained values of $\beta_{LM}(\theta_{\text{pol}})$. Meanwhile, the OR-PAD can also be expanded as

$$I^{\text{LF}}(\theta_{\text{elec}}^{\text{LF}}, \varphi_{\text{elec}}^{\text{LF}}; \theta_{\text{pol}}) = \frac{1}{\sqrt{4\pi}} C_0(\theta_{\text{pol}}) \left| \sum_{l=0}^{l_{\max}} \sum_{m=-l}^{l} \alpha_{lm}(\theta_{\text{pol}}) Y_{lm}(\theta_{\text{elec}}^{\text{LF}}, \varphi_{\text{elec}}^{\text{LF}}) \right|^2, \tag{11}$$

where $\alpha_{lm}(\theta_{\text{pol}})$ is a complex expansion coefficient, l is the orbital angular momentum of an electron being emitted, and m is the projection of l onto the $\boldsymbol{E}$-field (Z') direction. In Eq. (11), the spherical harmonics are regarded as the basis functions of the angular part of the photoelectron wavefunction, corresponding to the partial wave. Therefore, if we obtain the expansion coefficients $\{\alpha_{lm}(\theta_{\text{pol}})\}$, the physical meaning of the OR-PAD can be discussed in terms of the outgoing photoelectron wave function.

Because Eq. (11) can be expanded as

$$I^{\text{LF}}(\theta_{\text{elec}}^{\text{LF}}, \varphi_{\text{elec}}^{\text{LF}}; \theta_{\text{pol}}) = \frac{1}{\sqrt{4\pi}} C_0(\theta_{\text{pol}}) \sum_{l_1=0}^{l_{\max}} \sum_{l_2=0}^{l_{\max}} \sum_{m_1=-l_1}^{l_1} \sum_{m_2=-l_2}^{l_2} \alpha_{l_1 m_1}(\theta_{\text{pol}}) \alpha_{l_2 m_2}^*(\theta_{\text{pol}}) Y_{l_1 m_1}(\theta_{\text{elec}}^{\text{LF}}, \varphi_{\text{elec}}^{\text{LF}}) Y_{l_2 m_2}^*(\theta_{\text{elec}}^{\text{LF}}, \varphi_{\text{elec}}^{\text{LF}}), \tag{12}$$

$\beta_{LM}(\theta_{\text{pol}})$ in the expansion, Eq. (1), can be represented using as the coefficients, $\{\alpha_{lm}(\theta_{\text{pol}})\}$, using the Wigner's $3j$ symbols [29] as

$$\beta_{LM}(\theta_{\text{pol}}) = \frac{\sqrt{4\pi}}{C_0(\theta_{\text{pol}})} \int_0^\pi \int_{-\pi}^\pi I^{\text{LF}}(\theta_{\text{elec}}^{\text{LF}}, \varphi_{\text{elec}}^{\text{LF}}; \theta_{\text{pol}}) Y_{LM}^*(\theta_{\text{elec}}^{\text{LF}}, \varphi_{\text{elec}}^{\text{LF}}) \sin\theta_{\text{elec}}^{\text{LF}} \, d\theta_{\text{elec}}^{\text{LF}} \, d\varphi_{\text{elec}}^{\text{LF}}$$

$$= (-1)^M \sum_{l_1=0}^{l_{\max}} \sum_{l_2=0}^{l_{\max}} \sqrt{(2l_1+1)(2l_2+1)(2L+1)} \begin{pmatrix} l_1 & l_2 & L \\ 0 & 0 & 0 \end{pmatrix} \sum_{m_1=-l_1}^{l_1} \sum_{m_2=-l_2}^{l_2} \alpha_{l_1 m_1}(\theta_{\text{pol}}) \alpha_{l_2 m_2}^*(\theta_{\text{pol}}) \begin{pmatrix} l_1 & l_2 & L \\ m_1 & m_2 & -M \end{pmatrix}, \tag{13}$$

where $l_{\max}$ is set to be $l_{\max} = L_{\max}/2 = 2$. Note that the coefficients $\{\alpha_{lm}(\theta_{\text{pol}})\}$ satisfy the relation given by

$$\alpha_{l-m}(\theta_{\text{pol}}) = (-1)^m \alpha_{lm}(\theta_{\text{pol}}). \tag{14}$$

We set $\alpha_{00}(\theta_{\text{pol}})$ as a real value because only the relative phases of $\{\alpha_{lm}(\theta_{\text{pol}})\}$ is considered. Equation (13) represents the 15 simultaneous equations ($L \leqslant 4$, $0 \leqslant M \leqslant L$) in terms of the one real-valued variable, $\alpha_{00}(\theta_{\text{pol}})$, and five complex-valued variables, $\{\alpha_{lm}(\theta_{\text{pol}})\}(l = 1, 2, 0 \leqslant m \leqslant l)$, indicating that the set of these equations is overdetermined. The $|\alpha_{lm}(\theta_{\text{pol}})|$ and $\arg[\alpha_{lm}(\theta_{\text{pol}})]$ values at $\theta_{\text{pol}} = 85°$ are obtained by the least-squares analysis using Eq. (13) as shown in Figs. 13(a) and 13(b), respectively. The OR-PADs reconstructed from $\alpha_{lm}(\theta_{\text{pol}})$ in the energy ranges of $E_{\text{elec}} = 0.8$–1.2 eV and $E_{\text{elec}} = 0.2$–0.6 eV are shown in Figs. 13(c) and 13(d), respectively, which are in good agreement with the observed OR-PADs shown in Figs. 3 and 4. We note that the results of this partial wave analysis can be regarded as those obtained after averaging over the dihedral angle of 2π around the C-O axis because the dihedral angle of the C-O-H plane with respect to the $Z'X'$ plane is not specified in the present model.

In Fig. 13(a), $|\alpha_{00}(\theta_{\text{pol}})|$ and $|\alpha_{20}(\theta_{\text{pol}})|$ at $\theta_{\text{pol}} = 85°$ are much larger than the other $|\alpha_{lm}(\theta_{\text{pol}})|$ in both of the two energy regions, indicating that the photoelectron wavefunction is mainly composed of the s and d_0 waves. It is found that $\alpha_{l0}(\theta_{\text{pol}})$ with $m = 0$ are dominant over $\alpha_{lm}(\theta_{\text{pol}})$ with $m \neq 0$ in the entire range of θ_{pol}, reflecting the fact that $|\beta_{20}(\theta_{\text{pol}})|$ and $|\beta_{40}(\theta_{\text{pol}})|$ are much larger than the other $|\beta_{LM}(\theta_{\text{pol}})|$ as discussed in Sec. III D. In the case of tunneling ionization, the photoelectrons exhibiting a wavefunction with $m = 0$ are preferred to be emitted from the molecular orbital which contains the spherical harmonics with $m = 0$. This propensity for $m = 0$ observed in the OR-PADs suggests that the ionization proceeds via the tunneling ionization mechanism. By contrast, the fact that the photoelectron wave function can be described well by the spherical harmonics expansion of Eq. (11) with small orbital angular momenta of $l \leqslant 2$ in both of the two photoelectron energy regions suggests that the photoelectron emission proceeds in the multiphoton regime, which is consistent with the previous report [30] that the PAD contains the contribution from the large l values when tunneling ionization occurs so that a narrow angular range along the direction of the $\boldsymbol{E}$ field is realized. Therefore, it can
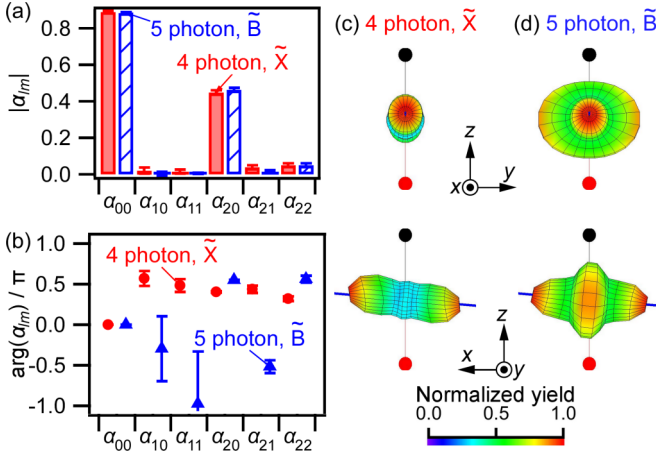
FIG. 13. (a) Magnitude of α_{lm} at $\theta_{pol} = 85°$. The red filled bars are for $E_{elec} = 0.8–1.2$ eV (the four-photon ionization to $\tilde{X}$) and the blue hatched bars are for $E_{elec} = 0.2–0.6$ eV (the five-photon ionization to $\tilde{B}$). (b) Arguments of α_{lm} at $\theta_{pol} = 85°$. The red circles are for the four-photon ionization to $\tilde{X}$, and the blue triangles are for the five-photon ionization to $\tilde{B}$. (c, d) OR-PADs at $\theta_{pol} = 85°$ reconstructed from α_{lm} for the four-photon ionization to $\tilde{X}$ and for the five-photon ionization to $\tilde{B}$, respectively. In these stereographic drawings, the yields are normalized by their maxima.

be said that the PADs obtained in the present study exhibit the characteristic features representing both the tunnel and multiphoton ionization schemes, which is consistent with the Keldysh parameters [31], $\gamma = 3.4$ and 4.1, for the ionization to $\tilde{X}$ and $\tilde{B}$, respectively, using the laser field intensity adopted in the present study. Indeed, it has been known for polyatomic molecules that multiphoton ionization and tunneling ionization coexist when the Keldysh parameter is moderately larger than 1.0 [32,33].

For the five-photon ionization to the $\tilde{B}$ state at $\theta_{pol} = 85°$, arg $[\alpha_{20}(\theta_{pol} = 85°)]$ takes a value of 0.55π, which is larger than $\pi/2$. This means that the real part of $\alpha_{20}(\theta_{pol} = 85°)$ is negative and that the s wave and the real part of the d_0 wave tend to interfere constructively at $\theta_{elec}^{LF} = 90°$ and destructively at $0°$ and $180°$. As a result, at $\theta_{pol} = 85°$, the photoelectron emission is enhanced in the direction perpendicular to the E field. According to the selection rule of the electric dipole transitions, in order that the s and d_0 waves are generated via the five-photon ionization by linearly polarized light, the molecular orbital from which an electron emitted needs to have spherical harmonic components having odd l and $m = 0$ such as the p_0 and f_0 components. As shown in Fig. 8(b), the $6a'$ molecular orbital, from which an electron is emitted in the five-photon ionization to the $\tilde{B}$ state, exhibits two lobes with their sign opposite to each other. This shape of the $6a'$ orbital, having the curved nodal surface perpendicular to the mirror plane of the C_S point group, contains the spherical harmonic components with odd l and $m = 0$ if the quantization axis (the E field) is perpendicular to the nodal surface. Therefore, when the E field is on the mirror plane and almost perpendicular to the C-O bond axis ($\theta_{pol} = 85°$), the E field is perpendicular to the nodal surface. Consequently, the photoelectrons can be emitted in the direction perpendicular to the E field, resulting from the constructive interference of the s and d_0 waves.

For the four-photon ionization to the $\tilde{X}$ state at $\theta_{pol} = 85°$, $|\alpha_{00}(\theta_{pol} = 85°)|$ and $|\alpha_{20}(\theta_{pol} = 85°)|$ are not largely different from those for the five-photon ionization to the $\tilde{B}$ state. However, arg $[\alpha_{20}(\theta_{pol} = 85°)]$ takes the value of 0.40π, which is smaller than $\pi/2$. This means that the real part of $\alpha_{20}(\theta_{pol} = 85°)$ becomes positive and that the s wave and the real part of the d_0 wave tend to interfere constructively at $\theta_{elec}^{LF} = 0°$ and $180°$ and destructively at $90°$. As a result, the photoelectron emission is enhanced in the direction parallel to the E field at $\theta_{pol} = 85°$. According to the selection rule of the electric dipole transitions, in order that the s and d_0 waves are generated via the four-photon ionization by linearly polarized light, the molecular orbital from which an electron emitted needs to have spherical harmonic components having even l and $m = 0$ such as the s and d_0 components. As shown in Fig. 8(a), the $2a''$ orbital, from which an electron is emitted in the four-photon ionization to the $\tilde{X}$ state, exhibits the d_1-like four-leaf clover shape whose quantization axis is perpendicular to the mirror plane of the C_S point group. Therefore, when the E field is perpendicular to the C-O bond axis, the ionization is expected to be suppressed because one of the two nodal planes of the $2a''$ orbital is almost perpendicular to the C-O bond. When the E field is parallel to the nodal plane, the photoelectron emission in the direction of the E field is suppressed through the destructive interference as discussed in Sec. III D. Indeed, as shown in Fig. 9(a), the ionization is suppressed when the E field is perpendicular to the C-O bond axis, which is consistent with the four-leaf clover shape of the $2a''$ orbital. Although the d_0 component at $\theta_{pol} = 90°$ cannot emerge in the $2a''$ orbital, the ionization probability $W(\theta_{pol})$ at $\theta_{pol} = 85°$ is not suppressed completely. The alignment angle estimated from the direction of the CH_3^+ recoil can be slightly deviated from the direction of the C-O axis at the moment of the photoelectron emission as described in Sec. III D. Even if the deviation angle from $\theta_{pol} = 90°$ is smaller than $10°$, the $2a''$ orbital can contain a nonnegligible d_0 component, resulting in the substantial ionization yield, as shown in Fig. 9(a).

Even though the value of arg $[\alpha_{20}(\theta_{pol} = 85°)] = 0.40\pi$ ($<\pi/2$) for the four-photon ionization to the $\tilde{X}$ state is smaller only by 0.15π than the value of arg $[\alpha_{20}(\theta_{pol} = 85°)] = 0.55\pi$ ($>\pi/2$) for the five-photon ionization to the $\tilde{B}$ state as described above, the PAD patterns are largely different from each other. This difference in the PADs is related to the sign of the real part of $\alpha_{20}(\theta_{pol} = 85°)$ for the four-photon ionization to the $\tilde{X}$ state and that for the five-photon ionization to the $\tilde{B}$ state, showing that the PAD pattern varies sensitively depending on the value of the complex expansion coefficients of $\{\alpha_{lm}(\theta_{pol})\}$.

IV. SUMMARY

By accumulating the coincidence events in which a photoelectron and a CH_3^+ fragment ions are produced from the dissociative ionization of methanol cation, $CH_3OH \rightarrow CH_3^+ + OH + e^-$, in a linearly polarized intense UV laser field (400 nm, 67 fs, 3.1×10^{13} W/cm^2), we have obtained the 3D momentum distribution for the electrons and that for the CH_3^+ ions and constructed the OR-PADs in the two kinetic energy ranges for the photoelectrons corresponding to
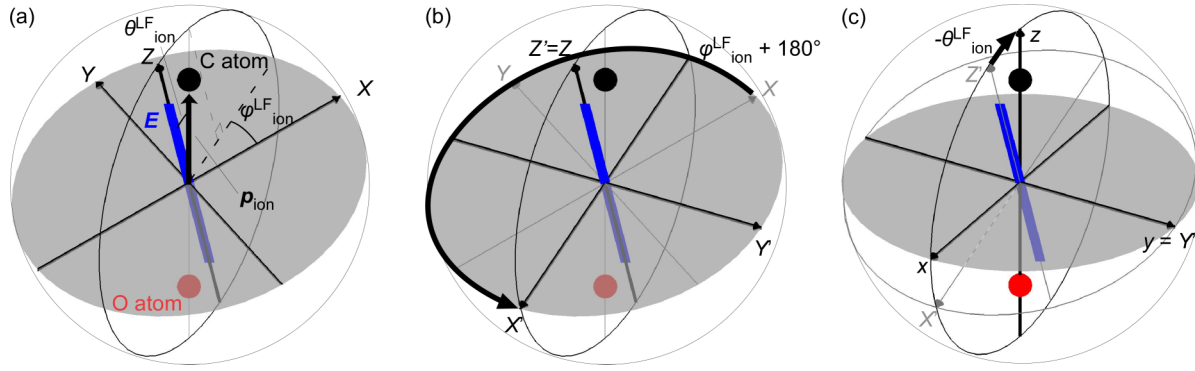
FIG. 14. Coordinate transformation for $0° \leqslant \theta_{\text{ion}}^{\text{LF}} \leqslant 90°$. When $90° \leqslant \theta_{\text{ion}}^{\text{LF}} \leqslant 180°$, $\theta_{\text{ion}}^{\text{LF}}$ is regarded as $(180° - \theta_{\text{ion}}^{\text{LF}})$. (a) The laboratory-frame (XYZ). (b) The OR-LF $(X'Y'Z')$ transformed by the rotation about the $Z(Z')$ axis by $(\varphi_{\text{ion}}^{\text{LF}} + 180°)$. (c) The OR-MF (xyz) transformed from the OR-LF by the rotation about the $Y'(= y)$ axis by $-\theta_{\text{ion}}^{\text{LF}}$.

the ionization to the $\tilde{X}$ and $\tilde{B}$ states. Based on the resultant OR-PADs, we have revealed how the direction of the photoelectron momentum $\boldsymbol{p}_{\text{elec}}$ is correlated with the direction of the $\boldsymbol{E}$ field as well as with the C-O axis. We have found that, in the four-photon ionization to the $\tilde{X}$ state, the photoelectrons are predominantly emitted along the $\boldsymbol{E}$-field direction and that, in the five-photon ionization to the $\tilde{B}$ state, the photoelectrons are emitted not only along the $\boldsymbol{E}$ field but also along the plane perpendicular to the $\boldsymbol{E}$ field. We have shown that this perpendicular component of the photoelectron emission becomes prominent as the polarization angle θ_{pol} increases from $5°$ to $85°$.

For more quantitative discussion, we have expanded the PADs into spherical harmonics in the orientation-angle resolved laboratory frame and have revealed that the photoelectrons tend to be emitted in the direction from the O atom to the C atom in the ionization to the $\tilde{X}$ state and in the direction from the C atom to the O atom in the ionization to the $\tilde{B}$ state at $\theta_{\text{pol}} = 5°$. We have also revealed that the direction of the photoelectron emission in the ionization to the $\tilde{X}$ state is shifted by $5°$–$10°$ from the $\boldsymbol{E}$ field towards the C-O bond at $\theta_{\text{pol}} = 45°$ and that the component of the photoelectron emission whose direction is perpendicular to the $\boldsymbol{E}$ field in the ionization to the $\tilde{B}$ state takes an elliptic-disk shape at $\theta_{\text{pol}} = 85°$.

In order to understand the physical meaning of the OR-PADs, we have expressed the PAD as the squared modulus of the expansion using spherical harmonics as described by Eq. (11), corresponding to the partial wave expansion. On the basis of this partial wave analysis and the dipole selection rule, we have shown that the characteristic photoelectron emission in the direction perpendicular to the $\boldsymbol{E}$ field at $\theta_{\text{pol}} = 85°$ can be interpreted by the constructive interference between the s and d_0 waves from the $6a'$ orbital for the five-photon ionization to the $\tilde{B}$ state and interpreted by the destructive interference between the s and d_0 waves from the $2a''$ orbital for the four-photon ionization to the $\tilde{X}$ state.

It should be noted that when molecules fixed in space are tunnel ionized in a circularly polarized laser field the recorded PAD in the MF has been regarded as an orientation-dependent ionization probability [34–41]. In the present study, we have

revealed how the PADs depends on the molecular orientation, reflecting the angular distribution of the molecular orbitals from which an electron is emitted, based on the OR-PADs recorded using the linearly polarized laser field whose intensity is in the intermediate range,

APPENDIX A: ORIENTATION-ANGLE RESOLVED FRAMES FOR DESCRIBING PHOTOELECTRON ANGULAR DISTRIBUTIONS

The direction of the momentum of CH_3^+, $\boldsymbol{p}_{\text{ion}}$, can be expressed by the polar coordinates $(\theta_{\text{ion}}^{\text{LF}}, \varphi_{\text{ion}}^{\text{LF}})$ in the laboratory-frame XYZ coordinate system whose Z axis is set to be parallel to the direction of the $\boldsymbol{E}$ field, i.e., the laser polarization direction, as shown in Fig. 14(a). In the case of $0 \leqslant \theta_{\text{ion}}^{\text{LF}} \leqslant 90°$, the XY coordinates are rotated about the Z axis by $\varphi_{\text{ion}}^{\text{LF}} + 180°$ to form the $X'Y'Z'$ coordinate system with $Z' = Z$ as shown in Fig. 14(b). Then, the $Z'X'$ coordinates are rotated about the Y' axis by $-\theta_{\text{ion}}^{\text{LF}}$ to form the xyz coordinate system with $y = Y'$, which represents the orientation-angle resolved molecular frame (OR-MF) with the $\boldsymbol{E}$ field lying on the zx plane, as shown in Fig. 14(c). Thus, the OR-MF xyz coordinate system shown in Figs. 14(c) and 15 is obtained by the Euler rotation of the laboratory-frame XYZ coordinate system shown in Fig. 14(a). By definition, the polar angle θ_{pol} of the $\boldsymbol{E}$-field direction on the zx plane measured from the z axis in the OR-MF is the same as $\theta_{\text{ion}}^{\text{LF}}$, that is, $\theta_{\text{pol}} = \theta_{\text{ion}}^{\text{LF}}$. Because of the reflection symmetry of the $\boldsymbol{E}$ field with respect to the plane perpendicular to the $\boldsymbol{E}$-field direction, $\theta_{\text{ion}}^{\text{LF}}$ in the range of $90° \leqslant \theta_{\text{ion}}^{\text{LF}} \leqslant 180°$ can be treated as $\theta_{\text{ion}}^{\text{LF}\prime} = (180° - \theta_{\text{ion}}^{\text{LF}})$ in the range of $0° \leqslant \theta_{\text{ion}}^{\text{LF}\prime} \leqslant 90°$, and by definition, the polar angle θ_{pol} of the $\boldsymbol{E}$-field direction is given by $\theta_{\text{pol}} = \theta_{\text{ion}}^{\text{LF}\prime}$.

We adopt the azimuthal angle φ_{elec} describing the angular correlation between $\boldsymbol{p}_{\text{elec}}$ and the laser polarization direction as shown in Fig. 15. In the OR-MF, using the
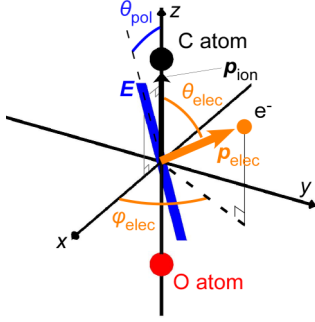
FIG. 15. Definitions of θ_{elec}, φ_{elec}, and θ_{pol} in the OR-MF with xyz coordinates. The z axis is set to be along the direction of the CH_3^+ recoil vector $\boldsymbol{p}_{ion}$ and the $\boldsymbol{E}$-field direction lies on the first and third quadrants of the zx plane.

polar and azimuthal angles, θ_{elec} and φ_{elec}, representing the direction of $\boldsymbol{p}_{elec}$, the orientation-angle resolved distribution of $\boldsymbol{p}_{elec}$, $f(p_{elec}, \theta_{elec}, \varphi_{elec}; \theta_{pol})$, in the volume element of $p_{elec}^2 \sin\theta_{elec}\, dp_{elec}\, d\theta_{elec} d\varphi_{elec}\, d\theta_{pol}$ is given by

$$f(p_{elec}, \theta_{elec}, \varphi_{elec}; \theta_{pol}) p_{elec}^2 \sin\theta_{elec}\, dp_{elec}\, d\theta_{elec}\, d\varphi_{elec}\, d\theta_{pol},$$

where $p_{elec} = |\boldsymbol{p}_{elec}|$. As long as the orientation angle θ_{pol} in the MF is defined on the zx plane on which the $\boldsymbol{E}$ field lies, we do not need to take account of the azimuthal angle of the $\boldsymbol{E}$ field and the corresponding factor of $\sin\theta_{pol}$ in the volume element. In other words, $f(p_{elec}, \theta_{elec}, \varphi_{elec}; \theta_{pol})$ includes implicitly the $\sin\theta_{pol}$ factor in the LF. When we

discuss the photoelectron yield, the θ_{pol} dependence has not been discussed. However, when we discuss the alignment-angle dependent ionization probability $W(\theta_{pol})$ shown in Fig. 9, which is plotted by the accumulated event numbers as a function of θ_{pol} in the LF, we need to take into account the volume element of $\sin\theta_{pol}$ as described by Eq. (2). In the energy-scaled polar coordinates, the distribution, $f_E(E_{elec}, \theta_{elec}, \varphi_{elec}; \theta_{pol})$, can be represented using $E_{elec} = p_{elec}^2/2$ and $dE_{elec} = p_{elec}\, dp_{elec}$ as

$$f_E(E_{elec}, \theta_{elec}, \varphi_{elec}; \theta_{pol})(2E_{elec})^{1/2}\sin\theta_{elec}\, dE_{elec}\, d\theta_{elec}\, d\varphi_{elec}$$
$$\times\, d\theta_{pol}.$$

Consequently, an OR-MF-PAD, $I(\theta_{elec}, \varphi_{elec}; \theta_{pol})$, is obtained by the integration of $f_E(E_{elec}, \theta_{elec}, \varphi_{elec}; \theta_{pol})$ over a specific range of E_{elec} between E_1 and E_2 as

$$I(\theta_{elec}, \varphi_{elec}; \theta_{pol}) \sin\theta_{elec}\, d\theta_{elec}\, d\varphi_{elec}\, d\theta_{pol}$$
$$= \left[\int_{E_1}^{E_2} f_E(E_{elec}, \theta_{elec}, \varphi_{elec}; \theta_{pol})(2E_{elec})^{1/2} dE_{elec}\right]$$
$$\times \sin\theta_{elec}\, d\theta_{elec}\, d\varphi_{elec}\, d\theta_{pol}. \tag{A1}$$

APPENDIX B: SPHERICAL HARMONIC EXPANSION OF OR-PAD

We expand the OR-MF-PADs by the spherical harmonics $Y_{LM}(\theta_{elec}, \varphi_{elec})$ as

$$I(\theta_{elec}, \varphi_{elec}; \theta_{pol}) = \frac{1}{\sqrt{4\pi}} C_0(\theta_{pol}) \sum_{L=0}^{L_{max}} \sum_{M=-L}^{L} \beta_{LM}^0(\theta_{pol}) Y_{LM}(\theta_{elec}, \varphi_{elec}), \tag{B1}$$

using the expansion coefficients $\beta_{LM}^0(\theta_{pol})$, where $\beta_{00}^0(\theta_{pol})$ ($L = M = 0$) is set to be 1. We adopt the Condon-Shortley phase [42] that is, a factor of -1 is adopted as the sign of the spherical harmonics only when M takes a positive odd value. The expansion coefficients, $\{\beta_{LM}^0(\theta_{pol})\}$, representing the anisotropy of the PADs, can be determined using the orthonormality of the spherical harmonics as

$$\beta_{LM}^0(\theta_{pol}) = \frac{\sqrt{4\pi}}{C_0(\theta_{pol})} \int_{-\pi}^{\pi} \left[\int_0^{\pi} I(\theta_{elec}, \varphi_{elec}; \theta_{pol}) Y_{LM}^*(\theta_{elec}, \varphi_{elec}) \sin\theta_{elec}\, d\theta_{elec}\right] d\varphi_{elec}. \tag{B2}$$

We confirm that, at $L_{max} = 4$, the expansion of Eq. (B1) converges to the best-fit distribution of the observed PAD in the entire range of θ_{pol}. We define the residual of the least-squares fit, $\delta(\theta_{pol})$, as a function of θ_{pol} as

$$\delta(\theta_{pol}) = \sqrt{\frac{\int_0^{\pi}\int_{\pi}^{-\pi}\left[\frac{1}{\sqrt{4\pi}}\sum_{L=0}^{L_{max}}\sum_{M=-L}^{L}\beta_{LM}^0(\theta_{pol})Y_{LM}(\theta_{elec}, \varphi_{elec}) - I(\theta_{elec}, \varphi_{elec}; \theta_{pol})\right]^2 \sin\theta_{elec}\, d\theta_{elec}\, d\varphi_{elec}}{\int_0^{\pi}\int_{\pi}^{-\pi}[I(\theta_{elec}, \varphi_{elec}; \theta_{pol})]^2 \sin\theta_{elec}\, d\theta_{elec}\, d\varphi_{elec}}}. \tag{B3}$$

We confirm that $\delta(\theta_{pol})$ becomes smaller than 0.2 for $\theta_{pol} \geqslant 15°$ and 0.3 for $\theta_{pol} = 5°$ as long as $L_{max} \geqslant 4$. At $\theta_{pol} = 5°$, the residual is larger than those at the other θ_{pol} values, because the accumulated event numbers are not sufficiently large at $\theta_{pol} = 5°$ due to the small solid angle range proportional to $\sin\theta_{pol}$. We further confirm that the residual decreases by ~ 0.1 when L_{max} is increased from 3 to 4, while it decreases only by a negligibly small amount of ~ 0.01 when L_{max} is increased from 4 to 5, which means that the convergence is

reached at $L_{max} = 4$ in the least-squares fit. Therefore, we adopt the results obtained with $L_{max} = 4$ in the following analysis.

The θ_{pol} dependence of the resultant coefficients, $\beta_{LM}^0(\theta_{pol})$, is found to be complicated. For example, in the four-photon ionization to $\tilde{X}$, $|\beta_{40}^0(\theta_{pol})|$ is the largest among $\{|\beta_{4M}^0(\theta_{pol})|\}$ ($L = 4$, $M = 0$, 1, 2, 3, 4) at $\theta_{pol} = 5°$ while $|\beta_{42}^0(\theta_{pol})|$ and $|\beta_{44}^0(\theta_{pol})|$ are the largest at $\theta_{pol} = 45°$ and $85°$, respectively, suggesting implicitly that the PADs tend

to be aligned to the laser polarization direction and that the OR-MF is not a good frame to describe photoelectron emission dynamics. In order to make the representation much more intuitive, we convert these coefficients of the OR-MF-PAD, $\{\beta^0_{LM}(\theta_{\text{pol}})\}$, into the expansion coefficients of the orientation-angle resolved laboratory frame (OR-LF) PAD, $\{\beta_{LM}(\theta_{\text{pol}})\}$. For example, in the OR-LF-PAD, $|\beta_{40}(\theta_{\text{pol}})|$ is more than three times larger than the other expansion coefficients, $|\beta_{4M}(\theta_{\text{pol}})|(M = 1, 2, 3, 4)$, in the entire range of θ_{pol}, as shown in Fig. 6(d).

The OR-LF-PAD, $I^{LF}(\theta^{LF}_{\text{elec}}, \varphi^{LF}_{\text{elec}}; \theta_{\text{pol}})$, is transformed from the OR-MF-PAD and is represented by Eq. (1). The

coefficients, $\beta_{LM}(\theta_{\text{pol}})(-L \leqslant M \leqslant L)$, of the OR-LF-PAD are described by a linear combination of $\beta^0_{LM'}(\theta_{\text{pol}})$ of the OR-MF-PAD having the same L as

$$\beta_{LM}(\theta_{\text{pol}}) = \sum_{M'=-L}^{L} \beta^0_{LM'}(\theta_{\text{pol}}) D^L_{M'M}{}^*(0, \theta_{\text{pol}}, 0), \qquad \text{(B4)}$$

where $D^L_{M'M}(0, \theta_{\text{pol}}, 0)$ is the Wigner's rotational matrix [29]. Note that the OR-MF-PAD and the OR-LF-PAD are equivalent and their coordinate systems can be converted from each other by the rotation about the $y = Y'$ axis because the orientation angle is specified.

[1] A. E. Boguslavskiy, J. Mikosch, A. Gijsbertsen, M. Spanner, S. Patchkovskii, N. Gador, M. J. J. Vrakking, and A. Stolow, The multielectron ionization dynamics underlying attosecond strong-field spectroscopies, Science **335**, 1336 (2012).

[2] K. Hosaka, A. Yokoyama, K. Yamanouchi, and R. Itakura, Correlation between a photoelectron and a fragment ion in dissociative ionization of ethanol in intense near-infrared laser fields, J. Chem. Phys. **138**, 204301 (2013).

[3] B. K. McFarland, J. P. Farrell, P. H. Bucksbaum, and M. Guhr, High harmonic generation from multiple orbitals in N_2, Science **322**, 1232 (2008).

[4] O. Smirnova, Y. Mairesse, S. Patchkovskii, N. Dudovich, D. Villeneuve, P. B. Corkum, and M. Y. Ivanov, High harmonic interferometry of multi-electron dynamics in molecules, Nature (London) **460**, 972 (2009).

[5] L. J. Frasinski, K. Codling, P. Hatherly, J. Barr, I. N. Ross, and W. T. Toner, Femtosecond Dynamics of Multielectron Dissociative Ionization by Use of Picosecond Laser, Phys. Rev. Lett. **58**, 2424 (1987).

[6] E. Shigemasa, J. Adachi, M. Oura, and A. Yagishita, Angular Distributions of $1s\sigma$ Photoelectrons from Fixed-In-Space N_2 molecules, Phys. Rev. Lett. **74**, 359 (1995).

[7] F. Heiser, O. Geßner, J. Viefhaus, K. Wieliczek, R. Hentges, and U. Becker, Demonstration of Strong Forward-Backward Asymmetry in the $C1s$ Photoelectron Angular Distribution from Oriented CO Molecules, Phys. Rev. Lett. **79**, 2435 (1997).

[8] J. A. Davies, R. E. Continetti, D. W. Chandler, and C. C. Hayden, Femtosecond Time-Resolved Photoelectron Angular Distributions Probed during Photodissociation of NO_2, Phys. Rev. Lett. **84**, 5983 (2000).

[9] Y. Tang, Y.-I. Suzuki, T. Horio, and T. Suzuki, Molecular Frame Image Restoration and Partial Wave Analysis of Photoionization Dynamics of NO by Time-Energy Mapping of Photoelectron Angular Distribution, Phys. Rev. Lett. **104**, 073002 (2010).

[10] C. Marceau, V. Makhija, D. Platzer, A. Y. Naumov, P. B. Corkum, A. Stolow, D. M. Villeneuve, and P. Hockett, Molecular Frame Reconstruction Using Time-Domain Photoionization Interferometry, Phys. Rev. Lett. **119**, 083401 (2017).

[11] V. Kumarappan, L. Holmegaard, C. P. J. Martiny, C. B. Madsen, T. K. Kjeldsen, S. S. Viftrup, L. B. Madsen, and H. Stapelfeldt, Multiphoton Electron Angular Distributions from Laser-Aligned CS_2 Molecules, Phys. Rev. Lett. **100**, 093006 (2008).

[12] Huynh Van Sa Lam, T. N. Wangjam, and V. Kumarappan, Alignment dependence of photoelectron angular distributions in the few-photon ionization of molecules by ultraviolet pulses, Phys. Rev. A **105**, 053109 (2022).

[13] X. Gong, P. He, Q. Song, Q. Ji, K. Lin, W. Zhang, P. Lu, H. Pan, J. Ding, H. Zeng *et al.*, Pathway-resolved photoelectron emission in dissociative ionization of molecules, Optica **3**, 643 (2016).

[14] S. Fukahori, M. Nakano, K. Yamanouchi, and R. Itakura, Channel-specific photoelectron angular distribution in laboratory and molecular frames for dissociative ionization of methanol in intense ultraviolet laser fields, Chem. Phys. Lett. **672**, 7 (2017).

[15] T. Ando, A. Shimamoto, S. Miura, K. Nakai, H. Xu, A. Iwasaki, and K. Yamanouchi, Wave packet bifurcation in ultrafast hydrogen migration in CH_3OH^+ by pump-probe coincidence momentum imaging with few-cycle laser pulses, Chem. Phys. Lett. **624**, 78 (2015).

[16] E. Herbst, J. K. Messer, F. C. De Lucia, and P. Helminger, A new analysis and additional measurements of the millimeter and submillimeter spectrum of methanol, J. Mol. Spectrosc. **108**, 42 (1984).

[17] K. Kimura, S. Katsumata, Y. Achiba, T. Yamazaki, and S. Iwata, *Handbook of HeI Photoelectron Spectra of Fundamental Organic Molecules* (Japan Scientific Societies Press, Tokyo, 1981).

[18] L. Karlsson, R. Jadrny, L. Mattsson, F. T. Chau, and K. Siegbahn, Vibrational and vibronic structure in the valence electron spectra of CH_3X molecules (X = F, Cl, Br, I, OH), Phys. Scr. **16**, 225 (1977).

[19] P. Warneck, Photoionisation von Methanol und Formaldehyd, Z. Naturforsch. A **26**, 2047 (1971).

[20] X.-M. Tong and S.-I. Chu, Density-functional theory with optimized effective potential and self-interaction correction for ground states and autoionizing resonances, Phys. Rev. A **55**, 3406 (1997).

[21] J. Muth-Böhm, A. Becker, and F. H. M. Faisal, Suppressed Molecular Ionization for a Class of Diatomics in Intense Femtosecond Laser Fields, Phys. Rev. Lett. **85**, 2280 (2000).

[22] J. Muth-Böhm, A. Becker, and F. H. M. Faisal, Erratum: Suppressed Molecular Ionization for a Class of Diatomics in Intense Femtosecond Laser Fields [Phys. Rev. Lett. **85**, 002280 (2000)], Phys. Rev. Lett. **96**, 039902(E) (2006).

[23] R. Itakura, P. Liu, Y. Furukawa, T. Okino, K. Yamanouchi, and H. Nakano, Two-body Coulomb explosion and hydrogen migration in methanol induced by intense 7 and 21 fs laser pulses, J. Chem. Phys. **127**, 104306 (2007).

[24] X. M. Tong, Z. X. Zhao, A. S. Alnaser, S. Voss, C. L. Cocke, and C. D. Lin, Post ionization alignment of the fragmentation of molecules in an ultrashort intense laser field, J. Phys. B: At. Mol. Opt. Phys. **38**, 333 (2005).

[25] K. I. Dimitriou, D. G. Arbó, S. Yoshida, E. Persson, and J. Burgdörfer, Origin of the double-peak structure in the momentum distribution of ionization of hydrogen atoms driven by strong laser fields, Phys. Rev. A **70**, 061401(R) (2004).

[26] M. Abu-Samha and L. B. Madsen, Photoelectron angular distributions from polar molecules probed by intense femtosecond lasers, Phys. Rev. A **82**, 043413 (2010).

[27] M. Bashkansky, P. H. Bucksbaum, and D. W. Schumacher, Asymmetries in Above-Threshold Ionization, Phys. Rev. Lett. **60**, 2458 (1988).

[28] J. Wu, M. Meckel, S. Voss, H. Sann, M. Kunitski, L. P. H. Schmidt, A. Czasch, H. Kim, T. Jahnke, and R. Dörner, Coulomb Asymmetry in Strong Field Multielectron Ionization of Diatomic Molecules, Phys. Rev. Lett. **108**, 043002 (2012).

[29] R. N. Zare, *Angular Momentum: Understanding Spatial Aspects in Chemistry and Physics* (Wiley, New York, 1988).

[30] B. Yang, K. J. Schafer, B. Walker, K. C. Kulander, P. Agostini, and L. F. DiMauro, Intensity-Dependent Scattering Rings in High Order Above-Threshold Ionization, Phys. Rev. Lett. **71**, 3770 (1993).

[31] L. V. Keldysh, Ionization in the field of a strong electromagnetic wave, Zh. Eksp. Teor. Fiz. **47**, 1945 (1964) [Sov. Phys. JETP **20**, 1307 (1965)].

[32] D. Mathur, T. Hatamoto, M. Okunishi, G. Prümper, T. Lischke, K. Shimada, and K. Ueda, Ionization of linear alcohols by strong optical fields, J. Phys. Chem. A **111**, 9299 (2007).

[33] R. J. Levis and M. J. DeWitt, Photoexcitation, ionization, and dissociation of molecules using intense near-infrared radiation of femtosecond duration, J. Phys. Chem. A **103**, 6493 (1999).

[34] A. Staudte, S. Patchkovskii, D. Pavicic, H. Akagi, O. Smirnova, D. Zeidler, M. Meckel, D. M. Villeneuve, R. Dörner, M. Y. Ivanov, and P. B. Corkum, Angular Tunneling Ionization Probability of Fixed-in-Space H_2 Molecules in Intense Laser Pulses, Phys. Rev. Lett. **102**, 033004 (2009).

[35] H. Akagi, T. Otobe, A. Staudte, A. Shiner, F. Turner, R. Dörner, D. M. Villeneuve, and P. B. Corkum, Laser tunnel ionization from multiple orbitals in HCl, Science **325**, 1364 (2009).

[36] J. Wu, L. P. H. Schmidt, M. Kunitski, M. Meckel, S. Voss, H. Sann, H. Kim, T. Jahnke, A. Czasch, and R. Dörner, Multiorbital Tunneling Ionization of the CO Molecule, Phys. Rev. Lett. **108**, 183001 (2012).

[37] H. Akagi, T. Otobe, and R. Itakura, Deformation of an inner valence molecular orbital in ethanol by an intense laser field, Sci. Adv. **5**, eaaw1885 (2019).

[38] L. Holmegaard, J. L. Hansen, L. Kalhøj, S. L. Kragh, H. Stapelfeldt, F. Filsinger, J. Küpper, G. Meijer, D. Dimitrovski, M. Abu-samha *et al.*, Photoelectron angular distributions from strong-field ionization of oriented molecules, Nat. Phys. **6**, 428 (2010).

[39] D. Dimitrovski, M. Abu-samha, L. B. Madsen, F. Filsinger, G. Meijer, J. Küpper, L. Holmegaard, L. Kalhøj, J. H. Nielsen, and H. Stapelfeldt, Ionization of oriented carbonyl sulfide molecules by intense circularly polarized laser pulses, Phys. Rev. A **83**, 023405 (2011).

[40] J. L. Hansen, L. Holmegaard, L. Kalhøj, S. L. Kragh, H. Stapelfeldt, F. Filsinger, G. Meijer, J. Küpper, D. Dimitrovski, M. Abu-samha *et al.*, Ionization of one- and three-dimensionally-oriented asymmetric-top molecules by intense circularly polarized femtosecond laser pulses, Phys. Rev. A **83**, 023406 (2011).

[41] J. Maurer, D. Dimitrovski, L. Christensen, L. B. Madsen, and H. Stapelfeldt, Molecular-Frame 3D Photoelectron Momentum Distributions by Tomographic Reconstruction, Phys. Rev. Lett. **109**, 123001 (2012).

[42] E. U. Condon and G. H. Shortley, *The Theory of Atomic Spectra* (Cambridge University Press, Cambridge, 1935).